batteries

MDPI

Review

Mechanical Intrusion of Aged Lithium-Ion Batteries: Boundary-Condition Continuity, Trigger Definitions, and the Limits of Cross-Study Comparability

Richard Polzer [1,*], Carlos Antônio Rufino Júnior [1,2,3], Sergej Diel [1] and Hans-Georg Schweiger [1]

[1] CARISSMA Institute for Electric, Connected and Safe Mobility (C-ECOS), Technische Hochschule Ingolstadt, Esplanade 10, 85049 Ingolstadt, Germany
[2] School of Electrical and Computer Engineering, University of Campinas (UNICAMP), Av. Albert Einstein, 400, Campinas 13083-896, Brazil
[3] Interinstitutional Graduate Program in Bioenergy (USP/UNICAMP/UNESP), 330 Cora Coralina Street, Campinas 13083-896, Brazil
* Correspondence: richard.polzer@thi.de

Abstract

Indentation and crush tests are widely used as crash-relevant surrogates for mechanical intrusion in Lithium-Ion Batteries (LIBs), yet their interpretation still relies on macroscopic, binary pass/fail criteria established at the Beginning of Life (BoL). This neglects how calendar and cyclic degradation alter a cell's mechanical, thermal, and structural state before abuse, leaving the literature on aged cells apparently contradictory. This review establishes an aging-aware interpretive framework that separates three levels commonly conflated: the boundary conditions governing deformation, the study-specific criteria and evidence strength behind a declared electrical event, and the post-trigger hazard progression captured within the available monitoring window. A descriptive synthesis of 22 normalized fresh-to-aged comparisons from 13 primary studies shows no universal aging-driven shift of the reported comparison event toward earlier or later force–displacement states, with force and displacement changing in the same direction in only about half of the cases. An apparent format-associated displacement pattern is substantially attenuated when the pouch-cell displacement ratios are normalized by the respective initial cell thicknesses: the pouch-cell median displacement ratio decreases from 1.07 to approximately 1.00, and the remaining variation differs across aging routes and states of charge, although their individual contributions cannot be separated in the available dataset. Many apparent contradictions likewise stem from non-equivalent mechanical boundary conditions and trigger definitions, and continuity of confinement—especially for pouch cells aged under stack pressure and tested in a relaxed state—is identified as a frequently overlooked interpretive variable, although no controlled aged-cell study has yet isolated its contribution. An earlier-reported trigger does not necessarily imply a more severe outcome. We distill these requirements into a tier-resolved reporting checklist, providing a more rigorous and reusable basis for abuse-test interpretation, model development, and safety qualification of batteries intended for long service life and second-life deployment.

Keywords: lithium-ion batteries; mechanical intrusion; indentation; crush; aging; confinement continuity; cell-format-associated patterns; regulatory testing; diagnostics

Check for updates

Academic Editor: King Jet Tseng

Received: 6 July 2026
Revised: 27 July 2026
Accepted: 30 July 2026
Published: 1 August 2026

Copyright: © 2026 by the authors. Licensee MDPI, Basel, Switzerland. This article is an open access article distributed under the terms and conditions of the Creative Commons Attribution (CC BY) license.

1. Introduction

Mechanical intrusion is a central safety concern for Lithium-Ion Batteries (LIBs) in crash-relevant environments [1]. Indentation and crush tests, which simulate mechanical abuse, assess how deformation can compromise the separator, a thin porous membrane that prevents contact between the positive and negative electrodes and maintains electrical insulation [2]. When vehicle structures or pack components indent or compress a cell, even modest external displacements can cause the layered electrode–separator assembly to deform [1,3]. This local deformation may cause the separator to rupture, allowing direct electrode contact and thereby initiating an Internal Short Circuit (ISC) [4]. However, the measured macroscopic force–displacement response does not uniquely indicate when or where internal failure occurs [5,6]. Similar global responses can arise from different damage locations, specific separator-failure events, and various ISC pathways under similar loading conditions [7]. This ambiguity exists even in fresh cells and is expected to worsen with cell aging, as previous degradation may predispose the system to different failure mechanisms before abuse.

Substantial progress has been achieved in establishing a mechanistic baseline for fresh cells at the BoL, with studies demonstrating that intrusion response is highly sensitive to indenter geometry, loading rate, fixture constraint, State of Charge (SoC), temperature, and cell format. Microstructural analyses and poromechanical modeling have clarified key deformation and failure mechanisms under mechanical abuse [8–13]. However, most insights are derived from pristine test articles, while cells in actual service experience coupled electrochemical, thermal, and mechanical aging. This aging process modifies interphases, increases transport resistances, alters gas content, drives thickness evolution, and compromises the structural integrity of separators, coatings, and interfaces [14–18]. As electrified fleets remain in operation for extended periods, it is no longer scientifically rigorous or industrially viable to treat the intrusion of aged cells as a simple extension of fresh-cell qualification [19].

Aging is not limited to the loss of residual capacity. It fundamentally alters the cell's pre-abuse electrochemical, thermal, dimensional, and mechanical condition and thereby diminishes structural robustness [14]. The intrusion response results from the interaction between these intrinsic aging effects and extrinsic test parameters, which together govern deformation and failure progression. Therefore, comparisons between fresh and aged cells are meaningful only when interpreted within the specific boundary conditions that influence cell responses, necessitating meticulous experimental control for scientific validity.

A key methodological consideration is whether the mechanical state induced by service aging is maintained during subsequent abuse testing. This issue is particularly relevant for pouch cells, which are often aged under stack pressure or module-representative preload but typically tested after this preload is removed, thereby altering their confinement conditions. In contrast, hard-cased cells inherently retain casing constraints throughout both aging and abuse phases. Any discontinuity or mismatch in confinement between aging and testing stages is a potential source of bias that complicates direct comparisons of fresh and aged cell intrusion responses. Whether it actually contributes to the observed fresh-to-aged trends has not yet been isolated experimentally.

Current regulatory standards and industrial qualification protocols primarily rely on standardized intrusion tests conducted under severe operating conditions, often at elevated SoC, while systematically neglecting the influence of battery aging [20]. Although this approach offers practical simplicity, it does not resolve whether qualification procedures validated on fresh cells are applicable to in-service, aged cells, or if aging fundamentally alters the mechanical failure landscape in ways not addressed by existing frameworks.

Although extensive research exists on the mechanical abuse of fresh cells, empirical studies examining aged cells under indentation or crush loading remain limited and unevenly distributed. The literature disproportionately focuses on pouch-cell formats, with significantly fewer comparative analyses of cylindrical cells and only isolated mechanical studies of aged prismatic or aged Lithium Iron Phosphate (LFP) cells, none of which yet provides the paired, event-resolved fresh-to-aged force–displacement data required for a normalized comparison. Furthermore, the predominant reliance on macro-scale observables restricts the ability to directly relate threshold shifts to internal, layered damage evolution. Consequently, discrepancies reported across studies rarely indicate genuine physical contradictions but more often result from heterogeneity in experimental design, boundary conditions, failure criteria, and monitoring scope. This issue is exacerbated for aged cells, where limited observability and inconsistent post-event assessment may be mistakenly interpreted as intrinsic aging effects.

Although existing reviews provide valuable foundational context, they do not address the persistent challenge of cross-study comparability. Studies on battery aging clarify the mechanistic basis for differences between fresh and aged cells, but do not integrate the heterogeneous results from indentation and crush investigations into an intrusion-focused interpretive framework [21,22]. Reviews center on battery safety testing and regulatory standards, cataloging abuse specifications, procedural frameworks, and acceptance criteria, yet offer limited insight into how prior aging influences intrusion test interpretation or how variations in fixture constraints, failure criteria, and post-event surveillance affect inter-study alignment [23]. A synthesis that separates the mechanical testing context, the explicit comparison event, and the subsequent hazard response in evaluating aged-cell intrusion phenomena remains notably absent.

To address this gap, this review introduces a three-tier analytical framework. The first tier defines the boundary conditions—geometry, constraint, loading rate, SoC, temperature, and chemistry—that govern deformation and damage evolution. The second tier examines how aging changes the mechanical response up to the reported comparison event and how that event is identified from the available signals. The third tier evaluates the subsequent electrical and thermal evolution within the reported observation window. A comparable tier logic has been used in experimental safety-risk evaluation: Jia et al. [24], for example, separate ISC triggering risk, ISC mode, and the subsequent thermal-runaway consequence within a single controlled cell and test program. The present review adapts this logic for intrusion-specific comparison across heterogeneous studies on aged cells, treating confinement history, event-identification criteria and their evidential basis, and post-event observation windows as explicit comparison variables. Figure 1 summarizes the framework and the two central findings that structure this review: aging does not shift the reported comparison event in a universal direction (first gate), and the position of that event does not predict the post-event hazard severity (second gate). Table 1 positions the framework against representative existing approaches.

Table 1. Comparison of representative synthesis approaches.

Approach	Unit of Analysis	What the Approach Resolves	Remaining Limitation for Aged-Cell Intrusion Comparison
Experimental three-tier safety-risk evaluation [24]	One controlled cell type and test program	Separates ISC triggering risk, ISC mode, and thermal consequence	Does not harmonize heterogeneous studies or differing confinement histories

Table 1. *Cont.*

Approach	Unit of Analysis	What the Approach Resolves	Remaining Limitation for Aged-Cell Intrusion Comparison
Testing-method-sensitive safety assessment [25,26]	Multiple abuse methods under defined aging mechanisms	Resolves test-method and degradation-mechanism dependence	Not intrusion-specific; does not normalize mechanical markers across studies
Abuse-testing and standards reviews [20,23]	Standards and prescribed test procedures	Compares load cases, procedures, and acceptance criteria	Aging history and event-evidence strength are not integrated
Aging-mechanism and degradation reviews [21,22]	Degradation mechanisms across technologies	Explains why aged cells may differ from fresh cells	Does not provide event-resolved mechanical comparison
This review	Heterogeneous published intrusion studies on aged cells	Separates boundary-condition history, reported marker and evidence, and post-event observability	Remains descriptive because the available studies are heterogeneous and confounded

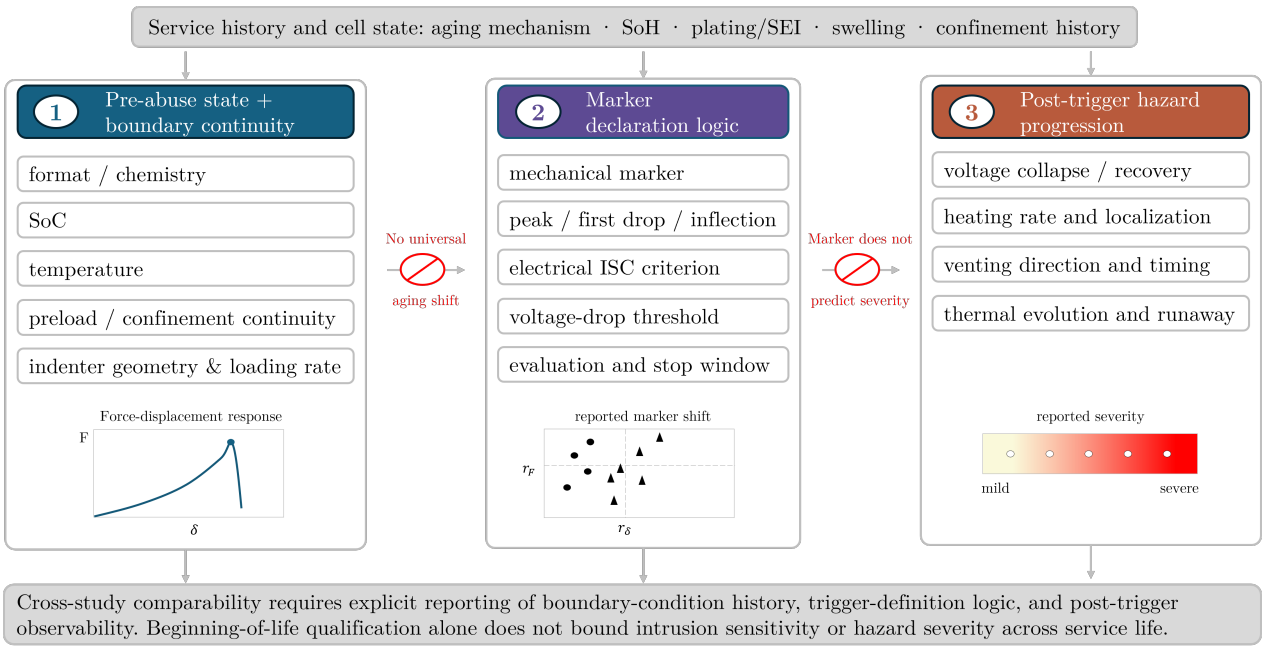

Figure 1. Three-tier framework separating the pre-abuse state and boundary conditions, marker declaration, and post-trigger hazard progression. Circles and triangles in the marker-shift schematic denote cylindrical- and pouch-cell comparisons, respectively. The red gates summarize the two central findings: no universal aging-driven marker shift and no direct relation between marker position and post-event severity.

This review limits its analytical scope to mechanical intrusion via indentation and crush loading, as these specifications serve as practical surrogates for crash-relevant mechanical tests [1]. Regulatory protocols and standards are referenced solely for their procedural relevance to intrusion qualification logic. Additional mechanical factors, such as vibration and shock, are considered only to contextualize intrusion phenomena within the broader battery safety framework [27]. In the surveyed literature, cell aging is defined as a capacity-based state of health (State of Health (SoH)) whenever such metrics are reported [28].

2. Scope and Methodology

This review examines the mechanical intrusion of aged LIBs subjected to indentation and crush loading. The methodological objective is to compare available evidence through a consistent interpretive framework that differentiates boundary conditions, study-specific comparison criteria, and post-event observations. The primary evidence base comprises studies that integrate mechanical abuse testing with prior aging of battery cells. The present section specifies how the evidence base was delimited, how terminology was harmonized across heterogeneous studies, and which metadata were recorded to support comparison of boundary conditions, reported comparison events, and post-event observations. When component tests on fresh and aged specimens accompany mechanical abuse testing, force–displacement curves are converted to engineering stress–strain, provided the specimen geometry required for transparent conversion is reported.

2.1. Terminology and Metadata Tracking

To ensure cross-study comparability, this review explicitly distinguishes between mechanically triggered events and electrically defined ISC criteria. Mechanical events refer to specific features on the force–displacement curve, including the initial force drop or peak force. In contrast, electrically defined criteria depend on changes in the cell's electrical response, primarily voltage drops, to identify an ISC, ideally synchronized with mechanical load data.

Because a voltage change during crush may also result from tab damage, terminal failure, intermittent contact, or measurement artifacts, an electrical signal alone does not prove internal electrode-to-electrode contact. Two distinct questions must therefore be separated: whether an ISC occurred at all in the test, and whether the timing of the declared electrical marker can be attributed to its onset. To make this explicit, each included case is assigned one of three levels of event-attribution evidence: E1—electrically detected event with no independent corroboration (a voltage change only), E2—ISC-consistent event, where the electrical signal is accompanied by concurrent evidence such as a localized temperature response at the intrusion site or a quantitative short-resistance estimate that makes an ISC plausible but does not confirm it, and E3—corroborated ISC occurrence, where thermal runaway, fire, post-test inspection, or imaging confirms that an internal short circuit took place. We stress that E3 corroborates the occurrence of an ISC but does not by itself establish that the declared electrical marker coincides with its onset. A time-resolved attribution of the onset, for example through in situ imaging, interrupted tests, or a validated synchronized model, is a stronger and currently rare form of evidence. Accordingly, the terms declared event and post-event are used where the attribution is E1 or heterogeneous across the compared cases, the phrase source-declared ISC-related event is used for E2, and the unqualified term ISC is reserved for E3, where the occurrence is corroborated. The event-attribution level of each case is documented in the study-level synthesis presented in Section 5.

During data extraction, relevant metadata were recorded, with missing values marked as "n.r.". The tracked parameters were categorized into experimental conditions (indenter geometry, confinement, loading rate, temperature), cell specifications (format, chemistry, SoC), and aging history (aging temperature, SoH, mechanical preload). Additionally, used electrical signals, failure or ISC onset definitions, stop criteria, observation periods, and final abuse outcomes (e.g., venting, fire, peak temperature, gas or mass loss, or Thermal Runaway (TR)) were documented.

2.2. Literature Selection and Synthesis Logic

The evidence base was compiled through a critical synthesis that integrated explicit aging information with mechanical intrusion loading.

The process commenced with a scoping step to refine the boundary-condition vocabulary used throughout the review, encompassing fixture and constraint history, indenter and contact conditions, loading rate, SoC, and temperature. Subsequently, targeted database searches were conducted across major publisher and platform databases, complemented by citation chaining. Figure 2 summarizes the workflow.

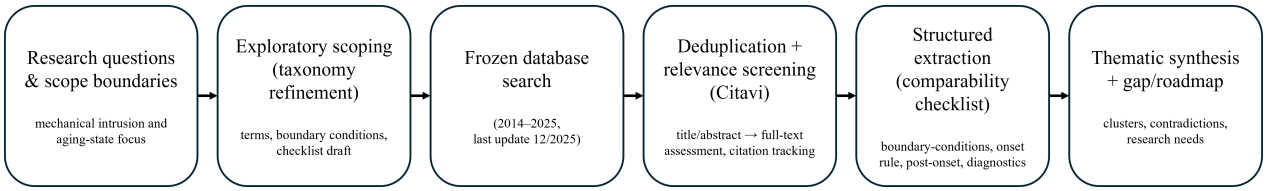

Figure 2. Literature-selection and synthesis workflow.

Database searches were conducted across major publisher and platform databases, including ScienceDirect, SpringerLink, IEEE Xplore, MDPI, and Wiley Online Library, covering the period from 2012 onward. The formal database search was completed in December 2025 and was complemented by a targeted update and continued citation chasing through June 2026, which added one recently published primary study [29]. The synthesis was restricted to English-language full texts. Keyword blocks combined lithium-ion battery terms related to format or chemistry with three further term groups. The first group covered intrusion-relevant mechanical loading terms such as indentation, crush, intrusion, and bending. The second group covered aging or state descriptors including aging, aged, cycling, calendar, SoH, and lithium plating. The third group covered event or diagnostic terms such as short circuit, voltage drop, contact loss, Electrochemical Impedance Spectroscopy (EIS), and imaging. Backward and forward citation chasing identified relevant primary studies whose terminology did not conform to a single keyword template. The keyword groups stated above define the search vocabulary transparently without implying exhaustive coverage.

Records were imported into Citavi for reference management and to document selection notes and study-specific metadata. Duplicates were removed during this process. Because this work is a focused critical synthesis rather than a formally registered systematic review, no record-level screening counts are reported. Instead, the included evidence base is disclosed in full: every study that enters the quantitative marker-ratio or post-event severity datasets appears with its extracted metadata in the synthesis tables presented later in the manuscript and in Appendix A. Appendix A documents, in numerical order, confinement conditions (Table A1), thickness normalization (Table A2), robustness summaries (Table A3), integrated post-event classification (Table A4), and detailed post-event signatures (Table A5). Contextual studies are cited where they are used. The inclusion criteria distinguish three evidence streams. First, the mechanical-marker dataset comprises publications that (a) report an explicit aging protocol or SoH metric and (b) perform mechanical intrusion with paired fresh and aged force–displacement values at a study-defined comparison event. This dataset contains 13 primary publications yielding 22 fresh-to-aged comparisons. Second, the post-event dataset comprises those cases that additionally resolve at least one electrical or thermal observable after the declared event. Cases in which one of these domains is not resolved are retained but flagged accordingly (Section 6). Third, contextual evidence, such as standards, reviews of diagnostic methods, and mechanistic aging reviews, provided framing and identified missing reporting requirements but was

not considered equivalent evidence for aging-sensitive intrusion outcomes. Standards and regulatory documents constituted a separate evidence stream to establish the baseline vocabulary of test specifications, stop criteria, and pass/fail logic motivating Sections 3 and 4.

Reported metadata and outcomes from the included primary studies were compared using the tracking scheme defined in Section 2.1. Missing elements were explicitly flagged to prevent inaccurate comparisons. When a study provided paired fresh and aged values for force and displacement at the same study-specific comparison event, aged-to-fresh ratios were calculated for force and displacement. These ratios were used for descriptive synthesis only, using counts, medians, and ranges by cell format. No inverse-variance weighting, pooling, or significance testing was applied because the observations differ in trigger definitions, boundary conditions, and comparison events, and because some observations are not independent within studies. To check that the descriptive patterns are not artefacts of a few entries, the same medians and ranges were recomputed for meaningful subsets (peak-force markers only, artificially cycled versus field-aged cells, and with the present dataset excluded) and, so that studies contributing several conditions are not over-weighted, with each publication represented by a single summary value. The thickness-normalized displacement ratio of Section 5 was carried through the same subsets. These summaries are compiled in Table A3, and the per-comparison values together with the evaluation script are provided as Supplementary Materials (Files S1 and S2). Since the primary studies rarely provide a common basis for boundary conditions, comparison-event definitions, ISC onset definitions, stop criteria, and post-event observation windows, assigning a formal study-level risk-of-bias score would suggest a level of comparability unsupported by the evidence base. Therefore, these comparability limitations are documented through the aforementioned metadata tracking.

3. Standards Context and Mechanical Qualification Test Specifications

Mechanical qualification of LIBs is governed by regulations and standards at the cell, module, and pack levels. These documents specify abuse scenarios and pass/fail criteria.

Overview of Test Specifications

Abuse testing is commonly grouped into electrical, thermal, and mechanical categories, each representing different risk scenarios across the battery life cycle, including manufacturing, transportation, vehicle operation, and end-of-life handling [23]. Within the mechanical domain, standards and regulations cover indentation and crush, penetration, drop, vibration, and shock. Rather than attempting a uniform treatment of all mechanical test classes, this review concentrates on indentation and crush, because these test procedures are most directly connected to crash-related intrusion.

Table 2 shows that mechanical qualification is firmly embedded in international battery standards. At the same time, these frameworks are designed mainly to define external loading scenarios and compliance criteria, not to resolve the internal failure mechanisms that develop during those tests [30].

In standardized intrusion tests, cells are exposed to quasi-static or dynamic loading, for example in drop or impact configurations, until a specified limit is reached, such as force, displacement, or voltage response. The associated contact conditions cover a wide range, from highly localized penetration by sharp nails to more distributed compression by flat plates, cylindrical or hemispherical indenters, or multi-rod platens, as summarized in Figure 3.

Table 2. Coverage of selected battery qualification standards and regulations.

Regulation Standard	Level	Region	Mechanical							Thermal			Electrical		
			Vibration	Shock	Crush	Penetration	Drop	Rollover	Altitude	Thermal Shock	Overheat	Fire	Short Circuit	Overcharge	Overdischarge
UN 38.3 [31]	C, M, P	UN	X	X	X				X	X			X	X	X
GTR 20 [32]	(M, P), S	UN	X	X	X					X	X	X	X	X	X
ECE R100 [33]	(M, P), S	UN	X	X	X					X	X	X	X	X	X
ECE R136 [34]	(M, P), S	UN	X	X			X			X	X	X	X	X	X
SAE J2380 [35]	(C), M, P, S	US	X												
SAE J2464 [36]	C, M, P, S	US	X	X	X	X	X	X		X	X	X	X	X	X
SAE J2929 [37]	C, M, P, S	US	X	X	X		X	X		X	X	X	X	X	X
FreedomCAR [38]	(C, M), P, S	US	X	X	X	X	X	X		X		X	X	X	X
UL 2580 [39]	C, M, P, S	US	X	X	X	X	X	X			X	X	X	X	X
USABC [40]	C, M, P, S	US	X	X	X	X	X	X		X	X	X	X	X	X
IEC 62281 [41]	C, M, P, S	IEC	X	X	X		X		X	X			X	X	X
IEC 62660-2 [42]	C	IEC	X	X	X					X	X		X	X	X
IEC 62660-3 [43]	C	IEC	X	X	X					X	X		X	X	X
IEC 62133-2 [44]	C	IEC	X	X	X		X			X	X		X	X	X
ISO 6469-1 [45]	(M, P), S	ISO	X	X	X					X	X	X	X	X	X
GB 38031 [46]	C, M, P, S	China	X	X	X		X	X	X	X	X	X	X	X	X
AIS-048 [47]	C, M, P, S	India	X	X		X		X					X	X	
KMVSS 18-3 [48]	P, S	Korea					X					X	X	X	X

Notes: C = cell, M = module, P = pack, and S = system. An X indicates that the standard or regulation includes the corresponding test category; a blank cell indicates that no corresponding requirement was identified. The background shading groups mechanical, thermal, and electrical test categories.

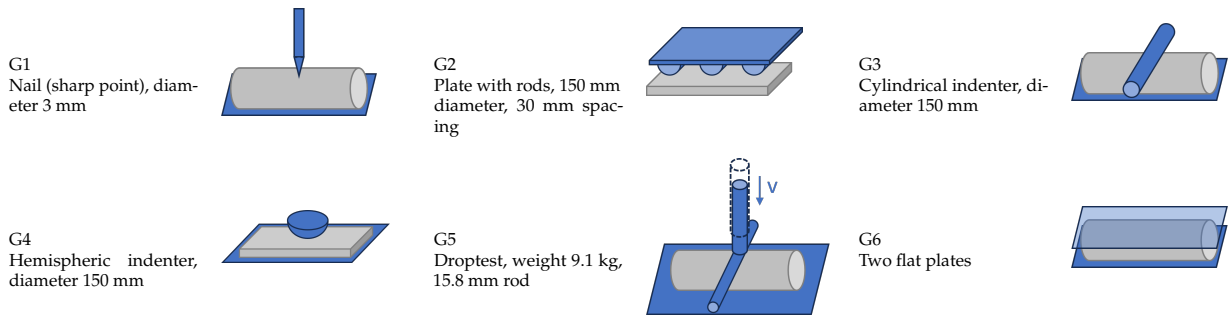

Figure 3. Representative indenter geometries and loading configurations used in cell-level indentation and crush testing.

Standards also differ substantially in their operational prescriptions. Table 3 compiles representative requirements for crush, penetration, and drop tests from selected standards. Despite ongoing harmonization efforts [49], notable differences remain in loading rate, prescribed SoC, temperature window, and stopping criteria.

The diversity of standards presents two immediate implications for evaluating aged cells:

1. Results are not inherently interchangeable. Setup choices determine distinct internal stress states and damage localizations [9], and stopping criteria influence reported outputs. Therefore, critical forces or displacement margins cannot be directly transferred across different cell formats and fixture concepts.
2. BoL is not a universal worst-case. Regulatory emphasis on fixed SoC states, particularly high or nominally severe BoL conditions, defines relevant certification scenarios. However, these setups do not necessarily capture the mechanically most critical state after aging-induced structural changes.

Table 3. Representative mechanical-test requirements in selected standards and regulations.

Regulation Standard	Speed mm s^{-1}	SoC %	Temp °C	Setting	Stop Criterion
SAE J2464 [36]	Dynamic 80	100	25 ± 5	Nail G1	Punch through
SAE J2464 [36]	Quasi Static 5–10	100	25 ± 5	Rod G3	Force 1000× cell weight Intrusion 50%
IEC 62660-2 [42]	Quasi Static Not specified	100	Room Temperature (RT)	Rod/Ball G3/G4	Force 1000× cell weight Voltage drop 1/3 Intrusion 15%
IEC 62133-2 [44]	Quasi Static Not specified	100	20 ± 5	Flat G6	Force 13 kN Voltage drop 1/3
IEC 62133-2 [44]	Dynamic	-	20 ± 5	Free fall 1 m on Flat	-
UN 38.3 [31]	Quasi Static	50	20 ± 5	Flat G6	Force 13 kN Voltage drop 100 mV Intrusion 50%
UN 38.3 [31]	Dynamic	50	Not specified	Drop 1 m G5	-
ECE R100 [33]	Dynamic Not specified	50	20 ± 10	Mult. Rods G2	Force 100 kN

Current BoL qualification should therefore be regarded as a necessary reference condition, but not as a complete basis for judging intrusion behavior over the full service life. If aging changes either the threshold for intrusion-induced failure or the severity of post-event escalation, additional aging-aware validation is needed to determine whether the BoL state still represents the bounding case. Building on this context, Section 4 systematizes how test boundary conditions physically modify the indentation and crush response, providing the foundation for synthesizing fresh-versus-aged shifts in reported comparison events in Section 5.

4. Boundary Conditions in Indentation and Crush Testing

Mechanical indentation and crush tests serve as crash-relevant surrogates at the cell, module, and pack levels. The mechanical stress state results from the interaction among cell architecture, indenter geometry, fixture constraints, loading rate, SoC, and cell or test temperature. Consequently, these boundary conditions influence the primary interpretive framework for comparing fresh and aged cell abuse results. Explicitly explaining these boundary descriptors reduces the risk of misattributing cross-study differences to aging when the underlying constraint history, loading mode, or thermal state are not aligned. Figure 4 summarizes the six boundary conditions treated in this section, showing the qualitative direction of their reported effects together with the key caveat that limits each direction.

A direction holds only together with the caveat in the last column — no boundary condition acts universally.

Boundary condition	Peak force F	Failure displ. δ	Post-trigger severity	Key caveat
Fixture, preload & confinement Section 4.1	↑	↓	–	Confinement must be equal during aging *and* abuse.
Cell chemistry & structure Section 4.2	–	–	high: LFP/NMC mild: LTO	Chemistry sets a ductile or brittle failure mode.
Loading geometry Section 4.3	–	↓ point ↑ flat	–	Depends on indenter shape and lateral support.
Strain rate Section 4.4	↑	↓	↑	The measured signal can differ from the real internal damage.
State of charge Section 4.5	↑ cyl. only	–	↑↑ thermal	Mechanical stiffening appears only in cylindrical cells.
Cell/test temperature Section 4.6	↓	↓	–	Strong under compression, weak in bending.

↑ increase ↓ decrease ↑↑ strong effect – no clear or emphasised effect

Figure 4. Qualitative synthesis of boundary-condition effects on peak force F, failure displacement δ, and post-trigger severity. Single arrows indicate a reported increase or decrease, whereas paired arrows indicate a strong reported effect. Dashes denote no clear effect, and gray labels denote categorical effects. The corresponding evidence is cited in the sections identified in the figure body. Each trend remains conditional on the caveat in the last column.

4.1. Fixture Constraints, Preload, and Confinement

The term confinement continuity refers to the retention of an equivalent mechanical constraint during both the aging and abuse phases, whereas confinement discontinuity indicates a change or release of this preload. This distinction is especially significant for pouch cells: out-of-plane restraint directly influences swelling evolution and inner layer support [50].

Höschele et al. [51] demonstrated the sensitivity of the global response to such constraints in fresh pouch cells. The application of out-of-plane preload and suppression of SoC-induced swelling altered the measured abuse response: increased confinement elevated initial stiffness and peak indentation forces, while electrically declared failure occurred at reduced indentation depths.

4.2. Cell Chemistry and Internal Structure

Cell chemistry affects both the mechanical failure mode and the resulting electrical and thermal outcome. Wang et al. [52] demonstrated this by comparing LFP, Nickel Manganese Cobalt Oxide (NMC), and Lithium Titanate (LTO) pouch cells under various indentation configurations. They observed that LFP and NMC cells show ductile crushing accompanied by pronounced separator collapse, resulting in rapid voltage drops. In contrast, LTO cells fractured in a brittle way with a delayed voltage decay and only mild temperature increases. This contrast likely reflects differences in the overall material constellation, including separator tensile behavior and electrode-level fracture characteristics, which together influence whether intrusion leads to progressive compaction or abrupt splitting.

The data indicates that chemistry influences the occurrence of failure and the manner in which internal damage manifests in externally observable signals. The main implication

is that apparent chemistry effects cannot be deduced solely from voltage or temperature traces without considering the underlying failure mode.

4.3. Loading Geometry and Boundary Conditions

Loading geometry determines the degree of deformation localization. In quasi-static indentation of cylindrical cells, Chung et al. [53] reported that localized contacts, such as spherical or rod indenters, are associated with earlier electrically observable failure during indentation. In contrast, distributed contacts, such as flat plates, trigger more global deformation prior to the detection of electrical failure.

Cross-study comparability depends in addition on whether the cell is laterally supported, permitted to rotate, or subjected to off-center loading. Zhu et al. [54] highlight that minor alignment variations can shift the dominant deformation mode, thereby modifying the observed ISC behavior. They propose that comparing a concise set of representative geometries enhances transferability across studies, for example, by combining rounded and localized contacts and supplementing indentation with four-point bending. Consequently, apparent differences between cell formats should not be inferred solely from force or displacement values unless the intrusion geometry produces comparable internal stress states.

4.4. Strain-Rate

Loading rate influences both the force–displacement response and the progression of failure. Furthermore, the presence of liquid electrolyte notably alters the measured mechanical behavior. Dixon et al. [55] demonstrated that, even within the quasi-static regime, pouch-cell intrusion varies considerably between wet production and dry surrogate cells. In aged cells, changes in electrolyte distribution [56] may serve as an additional confounding factor when interpreting rate effects.

Under dynamic loading, Kisters et al. [11,57] observed competing effects of strain-rate hardening and reduced ductility in pouch cells as impact velocity increased across a broad range. X-ray computed tomography revealed that higher velocities modify internal fracture topology, with cracks extending further from the intrusion center. Their analysis of the force–displacement response indicated that minor voltage changes may precede the force maximum, while the most significant voltage drop corresponds to later, more severe internal damage. The authors found that a pronounced voltage drop does not necessarily indicate a complete short circuit and that layer tearing can occur without a distinct macroscopic force signature. The primary implication for this review is that rate not only influences failure severity but can also decouple external signal interpretation from the actual internal damage state.

4.5. State-of-Charge

SoC influences mechanical intrusion behavior in two different ways. On the one hand, it can alter the mechanical response of the internal electrode–separator assembly prior to ISC by changing the electrochemically conditioned state of the cell. On the other hand, it determines how much electrical energy is available once internal contact has formed and therefore strongly affects the severity of subsequent thermal escalation.

For cylindrical 18,650 cells, this coupling to the mechanical response has been shown explicitly. Wang et al. [58] described a SoC-dependent constitutive response of the jellyroll and linked increasing SoC to an increasing resistance against deformation. In their compression tests, the peak force and corresponding displacement coincided with the reported electrical failure response.

For pouch cells, the influence appears differently. Deng et al. [59] reported very similar force–displacement curves for 20% and 100% SoC under impact, while only the temperature

response differed markedly: low-SoC cells heated only gradually, whereas fully charged cells showed rapid temperature increase and thermal runaway. In this case, SoC was therefore more evident in the post-failure thermal consequence than in the macroscopic mechanical response before failure.

Under dynamic loading, the effect of SoC is further overlaid by test configuration and cell format. Kotter et al. [60] found a pronounced strain-rate dependence in large-format prismatic cells but no significant SoC dependence in their dataset, while Zhang et al. [61] identified SoC as one of the factors affecting the force, electrical and thermal response as well as internal failure in impacted 18,650 cells.

Overall, the literature indicates that SoC is a relevant but not uniformly acting boundary condition. Its influence may appear in the mechanical and thermal response, depending on cell format and inherent cell constraint and loading scenario.

4.6. Cell and Test Temperature

Cell temperature influences mechanical intrusion primarily by shifting the mechanical response prior to severe electrical failure and, in some test configurations, by altering how mechanical and electrical markers relate to each other. Mo et al. [62] showed for 18,650 cells that under compression, increasing the temperature from 5 °C to 50 °C markedly reduced both the peak force and the displacement at which a short circuit was triggered. In the same study, however, three-point bending produced only minor temperature-dependent changes in peak force and displacement, and no short circuit occurred over the investigated temperature range. Temperature effects therefore did not act uniformly even within the same cell format, but depended strongly on the loading mode.

A related trend was reported by Gilaki et al. [63] for 18,650 cells tested between −40 °C and elevated temperatures. In both flat-plate crush and rod-indentation tests, increasing temperature reduced the failure load. However, the two configurations differed in how failure onset could be interpreted: in indentation, short circuit and mechanical failure occurred simultaneously and could be identified from the combined force–voltage response, whereas in flat-plate crush, early terminal failure prevented a clear voltage-based identification of internal short-circuit onset.

The available evidence indicates that mechanical abuse test temperature is mainly a pre-ISC boundary condition in the present context: it can shift the force level and displacement at the reported marker, but this effect is highly dependent on loading configuration.

Taken together, the boundary conditions outlined in Sections 4.1–4.6 establish the interpretive framework for assessing aging-related differences in mechanical intrusion. Reported changes in mechanical or electrical marker location, apparent intrusion tolerance, or post-marker severity are not comparable unless fixture constraint, loading geometry, SoC, temperature, and loading rate are adequately aligned or their variations explicitly stated. This framework underpins the subsequent synthesis of aging-dependent onset behavior and post-onset severity.

5. Mechanical Intrusion Tolerance Under Aging

Aging can shift the mechanically reported intrusion response of LIBs, but these shifts cannot be reduced to a single universal tolerance metric. At the same time, Section 4 has shown that indenter geometry, loading rate, SoC, temperature, fixture constraint, and cell format also reshape the force–displacement response and affect how electrical failure becomes detectable and declared. This section compares the study-specific shifts observed between fresh and aged cells under their respective abuse definitions and test configurations.

To enable the comparison across studies, two normalized descriptors are used: $r_F = F_{\text{aged}}/F_{\text{fresh}}$ and $r_\delta = \delta_{\text{aged}}/\delta_{\text{fresh}}$, where F and δ denote the reported force and

displacement at the study-specific point. Values greater than one indicate that the reported event occurs at higher force or larger intrusion in the aged condition, whereas values less than one indicate lower force or earlier occurrence. These ratios therefore describe directional shifts of the reported mechanical response within the stated experimental setup.

Figure 5 motivates why force and displacement ratios must be interpreted separately. Aging may shift a force–displacement response horizontally in displacement while simultaneously changing the force level at the selected comparison event. As a result, statements such as "aging reduces mechanical tolerance" are often too coarse. Force and displacement do not necessarily move in parallel, and similar curve shapes may still yield markedly different combinations of r_F and r_δ.

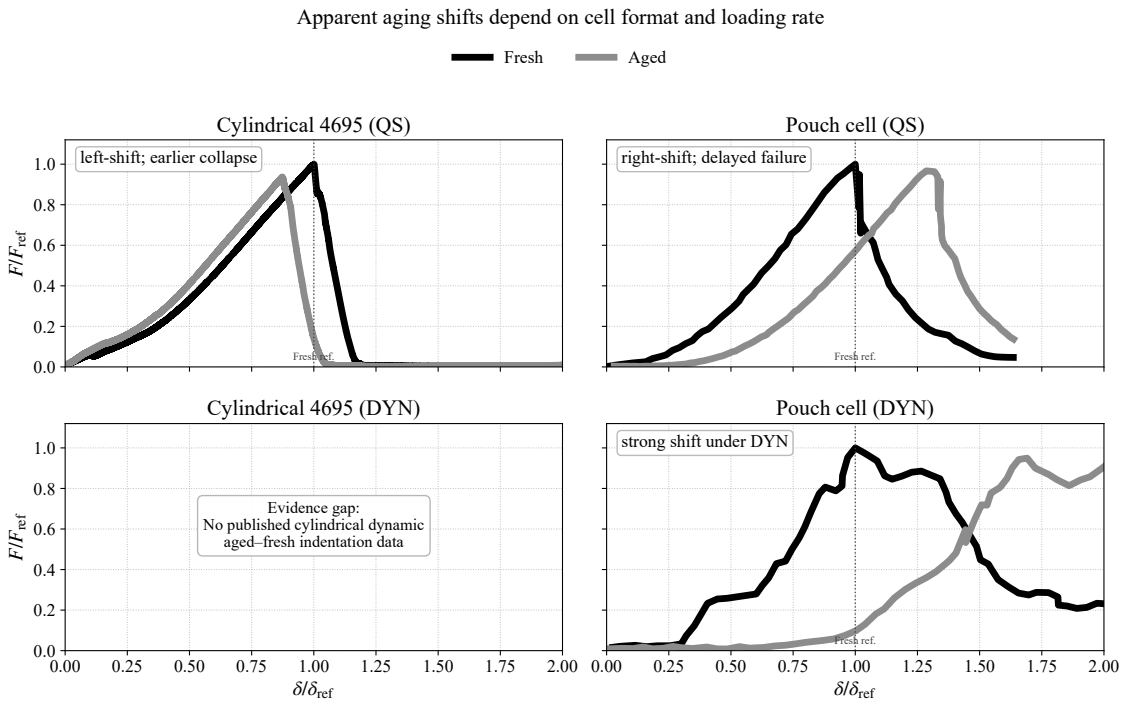

Figure 5. Peak-normalized force–displacement responses from representative pouch-cell studies [64] and the 4695 cylindrical-cell dataset [29]. The empty panel denotes the absence of a directly comparable aged–fresh cylindrical dataset under dynamic loading.

A central limitation for the interpretation of Section 5 is that the reported comparison event is not operationalized in a uniform way across the literature. This matters directly because the quantities compared in Table 4—for example F_{ISC}, δ_{ISC}, peak force, or first force drop—only become cross-study interpretable if the underlying trigger definition is transparent. Within the aged-cell abuse studies synthesized here, only Polzer et al. [29] explicitly define a reproducible electrical ISC criterion, identifying t_{ISC} as the earliest time at which the cell voltage exhibits a net drop of at least 50 mV within a sliding 0.10 s window. This permits a traceable mapping of the declared ISC onset onto force and displacement. In most of the remaining aged-cell studies, ISC is reported qualitatively or inferred from voltage behavior, but the exact signal-processing rule, threshold, or evaluation window is not specified. As a result, the reported mechanical state at ISC may correspond to different stages of electrical failure progression.

Table 4. Fresh-to-aged shifts in reported mechanical or ISC-linked markers.

Source	Cell	Cyclic Aging Condition	Abuse/BCs	Marker	Event Evid.	Ratios r_F/r_δ
Liu [65]	Pouch, NMC, 25 Ah	SoH 70% (at 0 °C)	QS, sphere 25 mm, SoC 25%	Peak force	E2	1.05/1.16
Liu [66]	Pouch, NMC, 25 Ah	SoH 70% (at 0 °C)	DYN, sphere 25 mm, 1 m/s, SoC 25%	First force peak	E3	n.r./1.00
Kovachev [67]	Pouch, NMC–LMO, 41 Ah	SoH 73% (at 60 °C)	QS, flat platen, SoC 100%	Peak force	E3	1.09/1.38
Qu [68]	Pouch, LCO, 4.12 Ah	SoH 70% (at 25 °C)	QS, sphere 13 mm, SoC 29–42%	Peak force	E2	1.02/1.23
Jia [24]	Pouch, NCMA, 3.2 Ah	300 cycles ≈SoH 98% (at RT)	QS, sphere 3 mm, SoC 20–100%	Peak force	E3	≈1.00/1.14
Spettmann [69]	Cyl. 18,650, NCA, 3.35 Ah	SoH 60% (at 0 °C)	QS, cyl. 15 mm, SoC 0%	ISC-related event	E2	0.89/0.74
Spettmann [69]	Pouch, NMC, 25 Ah	SoH 70% (at 0 °C)	QS, sphere 25.4 mm, SoC 0%	ISC-related event	E2	1.06/1.17
Sprenger [70]	Pouch, NMC, 74 Ah	SoH 90% (at −3–31 °C)	QS, cyl. 30 mm, SoC 0/100%	ISC-related event	E2/E3	SoC0: 0.71/1.07. SoC100: 1.00/1.50
Sprenger [64]	Pouch, NMC, 74 Ah	SoH 90% (at −3–31 °C)	DYN, cyl. 30 mm, SoC 0/100%	Electrical event	E1	SoC0: 0.94/1.07. SoC100: 1.06/1.60
Gstrein [71]	Pouch, NMC712/gr–SiO_x, 64.6 Ah	SoH 93% (field use)	QS, cyl. 30 mm, SoC 0/100%	Peak force	E2/E3	SoC0: 0.73/0.86. SoC100: 0.75/0.85
Abbas [72]	Pouch, NMC712/gr–SiO_x, 64.4 Ah	SoH 93% (field use)	QS, cyl. 30 mm, SoC 0/100%	Peak force	E2/E3	SoC0: 0.73/0.85. SoC100: 0.74/0.91
Abbas [72]	Pouch, NMC712/gr–SiO_x, 64.4 Ah	SoH 80% (at 10 °C)	QS, cyl. 30 mm, SoC 0/100%	Peak force	E2/E3	SoC0: 0.71/1.07. SoC100: 0.63/1.00
Guo [73]	Pouch, NMC/LMO, 2.5 Ah	SoH 70% (overcharge cycling, 4.65 V cutoff)	QS, sphere 10 mm, SoC 10%	Peak force	E2	0.93/1.29
Xu [74]	Cyl. 18,650, NCA (also LCO, LFP)	100 cycles (at RT)	QS, flat platen, SoC 0/40%	Peak force	E2	SoC0: 1.09/0.97. SoC40: 1.07/0.98
Polzer [29]	Cyl. 4695, NMC811/graphite, 30 Ah	SoH ≈ 80% (at −10 °C and 20 °C)	QS, sphere 50 mm, SoC 100%	ISC	E3	20 °C: 0.89/0.84. −10 °C: 0.81/0.78

Notes: Marker denotes the study-specific event used for fresh-to-aged comparison. Depending on the source, this may refer to a mechanically defined feature of the force-displacement response (e.g., peak point or peak force) or to force/displacement values evaluated at declared ISC occurrence. Consequently, r_F and r_δ remain tied to that reported marker and are not strictly identical threshold definitions across all studies. The Event evidence column gives the level of event-attribution evidence defined in Section 2.1: E1 = electrical anomaly only, E2 = temporally correlated multi-channel evidence, E3 = ISC occurrence corroborated. Combined levels (e.g., E2/E3) indicate that the level differs between the SoC or aging conditions within the row. Fresh and aged initial cell thicknesses and thickness-normalized displacement ratios are provided in Table A2.

Mechanical abuse studies on fresh cells help illustrate the extent of this problem. Kotter et al. [60], for example, define the critical state by a relative voltage-drop rule, namely a 2 % drop with respect to the floating average voltage over the preceding 5 % intrusion interval. Lamb and Orendorff [75] instead use a larger absolute event threshold of 100 mV and explicitly note that smaller voltage losses occurred earlier, such that a different threshold would have shifted the declared onset. Other studies classify outcomes only as minor or major ISC without reporting a quantified trigger rule. These studies remain valuable for understanding abuse behavior, but not all of them identify the same physical stage when they refer to ISC. For Section 5, this means that aging-induced shifts cannot be interpreted solely from the reported force or displacement value. They must be read together with the declaration logic by which the underlying event was defined.

The same caution applies to mechanical events. Across the literature, fresh-to-aged comparisons may be related to peak force, first peak, force-drop onset, or to force and displacement evaluated at an electrically declared ISC. Accordingly, the ratios listed in Table 4 remain tied to the event reported in each source. To adequately contextualize the observed shifts, the table details the cell format, indenter geometry, SoC, loading rate, and aging state, thereby preserving the distinct testing parameters of each study. Several mechanical abuse studies use an Inflection Point (IP) as an early indicator of a structural transition in the global mechanical response, rather than as direct proof of electrical failure [76]. The term is not used uniformly across publications. In multiple indentation studies, it is defined as the point of maximum stiffness in the global F–δ response, that is, a maximum in the local slope $dF/d\delta$ after smoothing or interpolation [65,68]. Xu et al. identify a related transition in nominal stress–strain space ("IP of $d\sigma/d\varepsilon$"), where the derivative peak may differ from the $dF/d\delta$-based definition when stress is normalized by a deformation-dependent contact area [74]. Spettmann et al. further show that for cylindrical cells voltage drops can occur at δ_{IP} before the first force peak, whereas pouch cells may lack a comparably distinct pre-peak transition, with voltage changes appearing only at or shortly after the peak [69]. In the present synthesis, IP is an example of how apparently similar onset statements may refer to different stages of mechanical progression.

Table 4 also makes the technology coverage of the compiled evidence explicit. The dataset already spans several high-nickel and next-generation chemistries—NMC811 [29], NCMA [24], and NCA [69,74] on the cathode side, and graphite–SiO_x silicon-bearing anodes in the two large field-aged pouch datasets [71,72]. Coverage nonetheless remains uneven, and the reason differs by technology. Fresh-cell work shows that cell chemistry alone can markedly change the mechanical, electrical, and thermal failure sequence: comparing LFP, NMC, and LTO cells under identical intrusion, Wang et al. [52] report material-system-dependent ductile versus brittle fracture modes, and SoC- and chemistry-dependent behavior is likewise documented for cylindrical NCA/LCO/LFP cells [74]. Aged LFP cells have also been studied mechanically: Wang et al. [77] characterize the out-of-plane compression and indentation response of aged prismatic LFP cells across SoH and independently attribute the right-shifted force–displacement curves of the aged cells to irreversible anode swelling and jellyroll stratification—consistent with the thickness mechanism of Section 5.2. That study does not, however, drive the aged cells to a declared electrical event and report paired fresh-to-aged force and displacement ratios, so it cannot enter the normalized comparison of Table 4. For aged prismatic, silicon-rich, solid-state, and lithium-metal cells the paired-state intrusion evidence required for the present normalization is currently absent or insufficient. Rather than synthesizing incomparable results to fill these gaps, these systems are identified as dedicated research targets in Section 7. Table 5 summarizes this coverage and locates the remaining gaps.

Table 5. Technology coverage of the compiled aged-cell intrusion evidence.

Technology	Paired Aged-vs-Fresh, Event-Resolved	Other Mechanical Intrusion Evidence	Representative Sources
Graphite/NMC, LCO (pouch, cyl.)	✓	✓	[64–66,68,70]
High-Ni cathodes (NMC811, NCMA, NCA)	✓	✓	[24,29,69]
Graphite–SiO_x (Si-bearing) anodes	✓	✓	[71,72]
LFP (cylindrical, prismatic)	—	✓	[52,74,77]
Prismatic format (general)	—	✓	[77]
Silicon-rich/lithium-metal anodes	—	n.a.	—
Solid-state cells	—	n.a.	—

Notes: ✓ = available; — = not available; n.a. = not systematically assessed. Only studies reporting paired fresh-to-aged force and displacement values at a declared event enter the normalized synthesis. Xu et al. [74] include LFP cells but do not report a separate paired, event-resolved fresh-to-aged LFP ratio; the ratios used in the synthesis are taken from their NCA dataset.

5.1. Visual Synthesis of Aging-Induced Shifts

Figure 6 condenses the entries from Table 4 into a two-dimensional view of normalized force and displacement shifts. Each point corresponds to one table entry and therefore to one reported event under the stated setup. Numbers in parentheses indicate the SoC at the start of the mechanical test. The map is intentionally descriptive: it is meant to reveal directional tendencies while keeping the core underlying metadata visible. It shows where the literature places the reported fresh-to-aged comparison point under the stated setup, but not how severe the subsequent electrical or thermal evolution becomes.

Within the present dataset, the clearest visual tendency is a format-associated pattern in the reported displacement ratio: pouch-cell studies more frequently occupy the $r_\delta > 1$ region, whereas all cylindrical-cell entries lie at $r_\delta < 1$. As shown in Section 5.2, a substantial part of this apparent pattern is attributable to aging-induced growth of the initial cell thickness in pouch cells, and format, aging route, marker definition, and confinement history are fully confounded in the compiled dataset, so no general physical format effect can be derived from it. At the same time, the map shows that force and displacement do not shift in parallel. Larger intrusion can coincide with force loss, and near-unity force ratios may accompany substantial intrusion increases. The compiled data therefore do not support a one-dimensional statement such as "aged cells always fail earlier" or "aged cells always tolerate less intrusion." Rather, they indicate that aging can alter the reported load-bearing capacity and the intrusion level at the selected event in different and partly decoupled ways.

The contrast reported by Spettmann et al. [69] illustrates this clearly. Even under a shared low-temperature aging protocol, the aged pouch cell shifts toward larger intrusion, whereas the aged cylindrical cell shifts toward earlier occurrence and lower force at the declared ISC event. In the same study, the cylindrical cell exhibits voltage drops already at IP, whereas the pouch cell does not show an equally distinct pre-peak transition. This underscores that superficially similar onset statements may refer to different stages of internal progression.

The compiled entries further show that SoC and loading rate can branch the apparent aging trend even within the same cell. For a 74 Ah pouch cell under cylindrical indentation, Sprenger et al. demonstrate that aging affects force and intrusion differently depending on SoC. Under quasi-static loading at SoC = 0%, the force at the reported marker decreases with aging, while the corresponding intrusion increases only slightly. At SoC = 100%, the intrusion ratio increases substantially, whereas the force ratio remains near unity [70].

Under dynamic loading, the force ratio can reverse direction between SoC levels, while the intrusion ratio increases at both SoC = 0% and 100% [64].

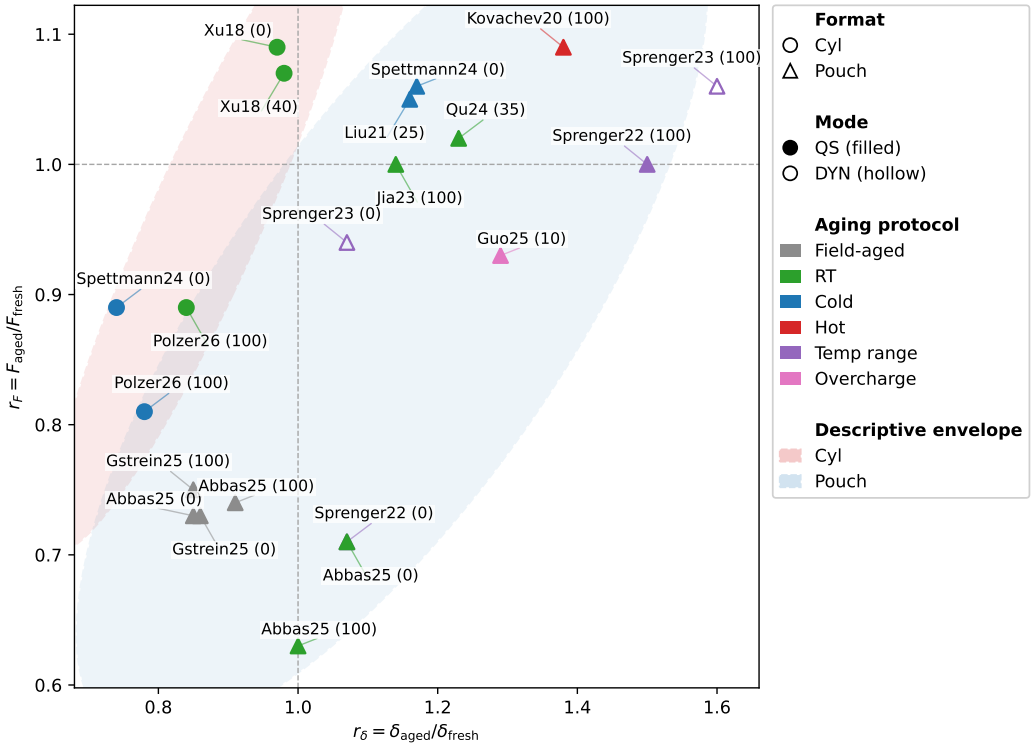

Figure 6. Normalized fresh-to-aged force and displacement ratios; parenthetical values indicate the test SoC (%).

Loading rate is similarly important because it can change what the reported marker represents mechanically. Using 25 Ah pouch cells and a spherical indenter, Liu et al. show that under quasi-static intrusion the relevant electrical event can coincide with the global peak force, whereas under dynamic intrusion ISC is triggered already at the first force peak and is frequently followed by partial voltage recovery [65,66]. Under dynamic loading, peak-based mechanical markers are less straightforward to interpret, and similar onset ratios can mask different internal progression.

The aging route itself constitutes a further branching variable beyond SoC and loading rate. For pouch cells aged by repeated slight overcharging to SoH 70%, Guo et al. report a peak-force reduction of 7% (4.58 kN to 4.28 kN) combined with a 29% larger peak displacement (2.20 mm to 2.84 mm) under spherical indentation [73]. The direction of this shift resembles the right-shifts observed for several conventionally cycled pouch cells, yet it arises from a distinct degradation pathway dominated by overcharge-induced side reactions. Conversely, early evidence on hard-cased elliptical cells indicates that cycling-induced separator degradation can move the declared onset in the opposite direction: separators extracted after extended cycling failed at lower punch force and smaller deformation, and the corresponding cell-level indentation tests showed reduced force and displacement at the onset of the short circuit after 1200 cycles [17]. Aging-route and component-degradation information is therefore required before a reported ratio pair can be attributed to a format- or chemistry-level trend.

Where reported, absolute values help to anchor these normalized ratios. For the field-aged 64 Ah pouch cells in Table 4, the aged-to-fresh comparison corresponds to peak forces dropping from 55.6 ± 1.2 kN to 41.4 ± 0.5 kN at 100% SoC and from 45.2 ± 0.4 kN to 33.2 ± 0.3 kN at 0% SoC, with failure displacements reduced by approximately 0.3 mm in both states [71]. For the lithium-plating-aged cells of the same type, the peak force decreases

to 36 ± 0.5 kN at 100% SoC while the failure displacement remains at 2.24 mm [72]. Such paired absolute values are currently the exception rather than the rule, which is one reason why the present synthesis operates on normalized ratios.

5.2. Initial Thickness and Thickness-Normalized Displacement Ratios

The displacement ratios compiled above are formed from absolute indenter travel referenced to first contact. For pouch cells, aging itself changes the initial cell thickness before any abuse loading is applied: the included studies report irreversible thickness increases between approximately 3% and 21% (see the source-level audit in Table A2). A larger absolute displacement at the reported event may therefore reflect a greater initial thickness rather than an improved intrusion tolerance. To assess how sensitive the observed displacement shifts are to differences in initial cell thickness, an initial-thickness–normalized displacement ratio is defined as

$$r_\varepsilon = \frac{\delta_{\text{aged}}/h_{\text{aged}}}{\delta_{\text{fresh}}/h_{\text{fresh}}} = \frac{r_\delta}{h_{\text{aged}}/h_{\text{fresh}}}, \tag{1}$$

where δ_{aged} and δ_{fresh} are the respective event displacements and h_{aged} and h_{fresh} are the corresponding initial cell thicknesses. The ratio r_ε compares nominal compression at the reported event instead of absolute travel. All nine pouch-cell source clusters provide sufficient thickness information for the normalization: six report absolute or approximate fresh and aged thickness pairs and three report a relative thickness change, so every pouch entry could be normalized. The same audit records the corresponding values and whether each input is absolute, read from a figure, or reported only as a relative change. No analogous normalization was applied to the cylindrical entries because aging-induced changes in outer diameter were not reported and the metallic casing strongly constrains radial expansion.

The normalization substantially attenuates the aggregate right shift. At the level of individual fresh-to-aged comparisons (17 pouch-cell comparisons from 11 publications), the median decreases from $r_\delta = 1.07$ to $r_\varepsilon \approx 1.00$. When each publication is given equal weight by first reducing its comparisons to a within-study median, the corresponding overall median decreases from $r_\delta = 1.17$ to $r_\varepsilon = 1.08$. To avoid over-interpreting values close to unity, ratios within ±5% of one ($0.95 \leq r \leq 1.05$) are treated as near-unity and not read as a directional shift. A ±10% band was checked as a sensitivity and does not change the qualitative reading. Under this near-unity rule, the number of pouch comparisons that remain above the band ($r > 1.05$) decreases from 11 to 8 of 17 (Table A3). Individual entries respond very differently: the quasi-static and dynamic SoC = 0% shifts of the 74 Ah pouch cell ($r_\delta = 1.07$) coincide almost exactly with the measured 6.3% thickness increase and reduce to near-unity ($r_\varepsilon \approx 1.00$) [64,70], and the overcharge-aged cell, which shows the largest reported initial-thickness increase in the compiled pouch dataset (20.7%), decreases from $r_\delta = 1.29$ to $r_\varepsilon = 1.07$ [73]. In contrast, the high-temperature-aged cell retains $r_\varepsilon = 1.29$ [67], and the SoC = 100% shifts of the 74 Ah cell remain at 1.31–1.40 [64,70]. The field-aged entries move further below unity (0.81–0.89) [71,72], and the lithium-plating-aged entries reduce to near-unity or just below (0.92–0.98) [72]. After normalization, the remaining variation differs across aging routes and test SoC conditions: artificially cycled cells tested at high SoC retain the clearest right shifts, whereas the field-aged entries shift left. Their individual contributions cannot be separated in the available dataset because aging route, SoC, cell design, and test conditions remain confounded.

This reading is consistent with the included sources themselves. Kovachev et al. explicitly attribute the displacement offset between fresh and aged curves ($\Delta x = 0.57$ mm) to the measured thickness increase of 0.55 mm and to the initial compaction of the thicker,

softer Solid Electrolyte Interphase (SEI) [67]. Sprenger et al. justify the increased failure displacement of their aged cells by "an increased cell thickness due to an additional softer layer" on the aged graphite [64], Guo et al. relate the increased peak displacement directly to the change in cell thickness [73], Abbas et al. describe the initial compaction of the soft plated-lithium layer before the response resembles the fresh cell [72], and Jia et al. report a nominal ISC strain $\varepsilon_{\mathrm{ISC}} = d_{\mathrm{ISC}}/h$ alongside the relative thickness change for exactly this reason [24]. Equation (1) assumes failure at equal nominal compression. The source-level interpretation of an initially compacted soft surface layer would correspond to an offset-type adjustment $\delta_{\mathrm{aged}} - \Delta h$ and would attenuate individual right-shifts even more strongly. This normalization therefore provides a sensitivity estimate of the thickness contribution rather than a geometry-independent measure of local failure strain: because δ/h is not directly comparable across spherical, cylindrical, and flat-platen indentation, contact area, lateral material flow, layer densification, friction, and boundary conditions still differ between entries.

Three caveats apply: one thickness pair is read from a published figure rather than a table [69], one is reported at an unspecified SoC while the abuse test was performed fully charged [67], and SoC-matched thickness pairs are only available for two sources [70,72]. The normalization consequently supports sensitivity statements rather than replacement of the reported values, and both r_δ and r_ε are reported side by side in Figure 7. Under the normalization, the marker-shift classification used in Section 6 is robust for 20 of 22 entries. Only the two lithium-plating-aged comparisons reclassify from a mixed to a lower-margin marker shift. Because no aged-cell study to date performs intrusion testing under retained aging preload, an experimental separation of the thickness contribution from genuine state changes remains outstanding (Section 5.4.1).

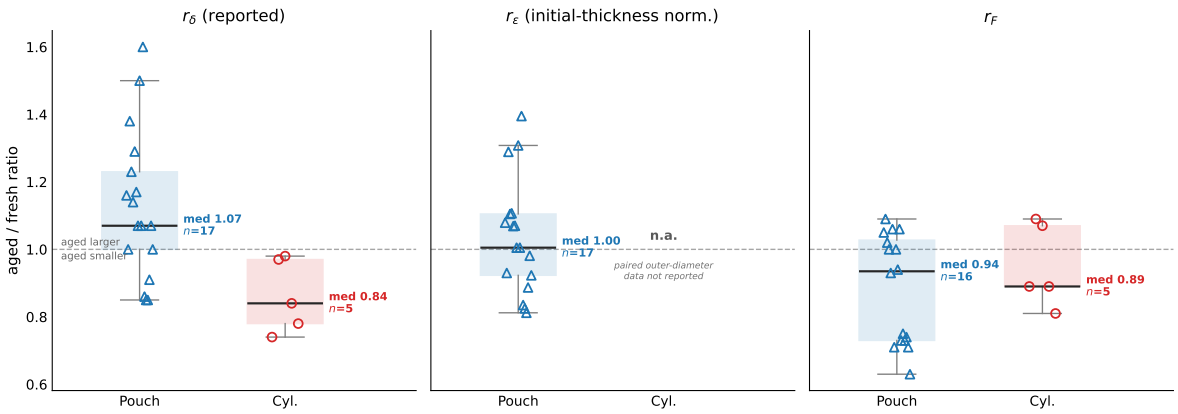

Figure 7. Distributions of r_δ, the pouch-cell thickness-normalized ratio r_ε, and r_F, grouped by cell format. Triangles denote pouch-cell comparisons, circles denote cylindrical-cell comparisons, and "Cyl." denotes cylindrical cells. Points represent individual comparisons; boxes show the median, interquartile range, and non-outlier range.

5.3. Descriptive Quantitative Synthesis of the Compiled Ratios

With the reported and thickness-normalized displacement ratios now defined, the compiled ratio pairs are summarized descriptively by cell format. The unit of observation is one reported fresh-to-aged comparison under one stated configuration. Several observations may originate from the same study, and the underlying markers are not identical across entries. The summary is therefore a structured description of the evidence base, not a meta-analysis, and the reported medians and ranges must not be read as estimates of a common underlying effect. Figure 7 visualizes the compiled values as non-parametric distributions grouped by cell format.

Three descriptive observations follow. First, the reported displacement ratios show an apparent format-associated pattern in this limited dataset: all five cylindrical entries lie at $r_\delta < 1$ (median 0.84), whereas the majority of pouch entries lie at $r_\delta > 1$ (median 1.07, with $r_\delta > 1$ in 11 of 17 pouch entries). The four field-aged pouch entries at $r_\delta < 1$ [71,72] already show that this pattern is not absolute, and the thickness normalization reduces the pouch median to approximately 1.00, so the apparent format-associated separation is substantially attenuated once aging-induced swelling, aging history, and confinement are accounted for rather than format alone. The cylindrical direction (all entries below unity) is robust as a directional statement, but its magnitude is dominated by two studies, including our own dataset [29,69], and should therefore not be read quantitatively. Second, the force ratio does not show a comparable pattern: both groups span values below and above unity, and the overall median of 0.93 indicates only a weak tendency toward reduced force at the reported marker. Third, force and displacement shifts are directionally concordant in barely more than half of the entries (12 of 21 as reported, 14 of 21 after thickness normalization), which quantitatively substantiates why one-dimensional statements about aged-cell "intrusion tolerance" are not supported: the two coordinates of the reported event frequently move in different directions.

5.4. Bias Sources and Transfer Limits

The ratios presented in Figure 6 do not resolve whether aging-related shifts are governed primarily by changes in boundary conditions and mechanical state or by intrinsic changes in separator and electrode response. This distinction is central to interpreting the map. The observed pouch–cylindrical contrast may reflect genuine format- and architecture-dependent aging effects, but it may also be amplified by systematic differences in constraint continuity between aging and abuse. Two possible bridging factors are therefore considered where supported by the literature: confinement history and component-level mechanical changes measured on extracted layers.

5.4.1. Confinement History and Mechanical Preconditioning of Pouch Cells

The apparent format contrast observed in the compiled ratios should not be interpreted as a pure format effect. Cylindrical cells typically retain external constraint through the rigid casing during both aging and subsequent abuse testing. In contrast, mechanical abuse studies on aged pouch cells commonly report flat-plate aging preload levels ranging from approximately 0.008 to 0.06 MPa, with values near 0.05 MPa most frequently documented [65–69,72]. Additional datasets involve aging within modules or field use, where geometric confinement exists and stack pressure is likely present, but is not actively controlled or reported [64,71]. Since the subsequent abuse tests are generally carried out without this preload, the structural state established during cycling may be only partially preserved at the onset of mechanical loading and not representative of in-service aging and mechanical loading, e.g., in a vehicle crash. It must be emphasized, however, that no controlled aged-cell study currently isolates retained versus released preload while holding the remaining test conditions constant. The available evidence shows that confinement affects the mechanical response of fresh cells [51], but not that confinement discontinuity explains the observed fresh-to-aged trends. The discontinuity is therefore treated here as a candidate mediator and potential source of bias. A detailed comparison of confinement during aging and subsequent abuse testing of pouch cells is provided in Table A1, which documents this evidence gap.

Figure 8 illustrates the above-mentioned logic: panel (a) depicts a confinement discontinuity in a pouch cell, Panel (b) presents the more persistent structural enclosure of a cylindrical cell, and Panel (c) shows a preload-retaining fixture concept [51] for pouch

cells. Therefore, boundary-condition transfer should be considered an explicit interpretive variable when comparing fresh against aged pouch or cylindrical cell responses.

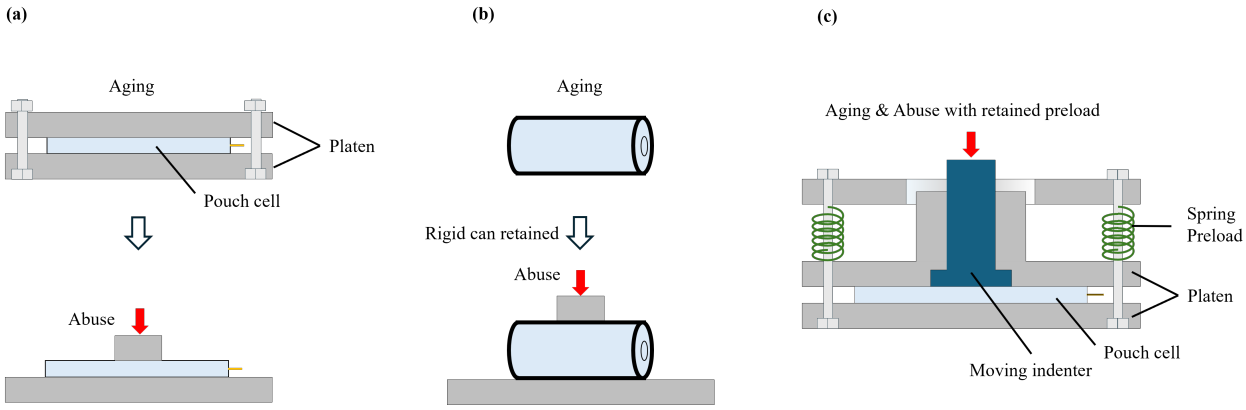

Figure 8. Boundary-condition transfer between aging and abuse: (**a**) pouch-cell aging under platen confinement followed by abuse after release of that confinement; (**b**) cylindrical-cell aging and abuse with the rigid can retained; and (**c**) a spring-preloaded pouch-cell fixture that maintains confinement during both aging and abuse, adapted from Höschele et al. [51].

5.4.2. Component-Level Mechanics

A limited subset of reviewed studies reports tensile and/or compressive tests on extracted separator and electrode specimens aged under the same conditions as those used in cell-level abuse experiments. To isolate the effects of aging from variations in test setups, this analysis focuses exclusively on studies that directly compare fresh and aged components [65,68,70,71]. Because each specimen is extracted and compared in the fresh and aged state directly, these tests are not affected by the confinement-transfer mismatch discussed in Section 5.4.1. There is no casing and no aging preload that could be released before loading, so any difference reflects a change in the material itself. In principle, the component scale is therefore the cleanest available window on the intrinsic material contribution to aging, and the natural place to ask whether the cell-level format contrast has a material origin. The decisive limitation is that all currently available extracted-component stress–strain datasets stem from pouch cells, so this window cannot by itself separate a pouch from a cylindrical material response. The aim here is accordingly the more modest one of qualitatively assessing aging-induced changes in stiffness, yield strength, and compaction behavior, and of testing whether their direction is even consistent with the compiled cell-level shifts.

Figure 9 shows that aging-related changes at the component scale are generally modest in the initial low-strain regime but become more pronounced in stronger hardening and compaction regimes.

Tension: For the anode, most datasets indicate slight aging-related softening, characterized by lower stress at a given strain and reduced apparent yield, although [71] reports an opposing trend. Cathode tensile curves largely overlap within each study, suggesting that fresh-to-aged differences are minor relative to inter-study variation in absolute stress levels. The separator shows the greatest divergence in reported aging effects: [65] reports nearly unchanged tensile behavior, whereas [70] observes markedly reduced initial stiffness and yield stress in aged specimens.

Compression: Under compression, both anode and cathode exhibit substantial inter-study variability, and aging-related deviations become more evident at higher strains, where densification and damage accumulation are expected to dominate. For the anode, the compiled datasets suggest that aging may cause a rightward shift and/or altered peak and softening behavior, but both the direction and magnitude vary across studies [65,68,70].

Some datasets terminate at relatively low stress or strain levels, which limits comparability in the regime where the curves diverge most strongly [71]. Cathode compression responses are similarly difficult to compare because of differing strain ranges and termination criteria. For separator compression, only [70] provides data, showing comparatively small fresh-to-aged differences over the examined strain range.

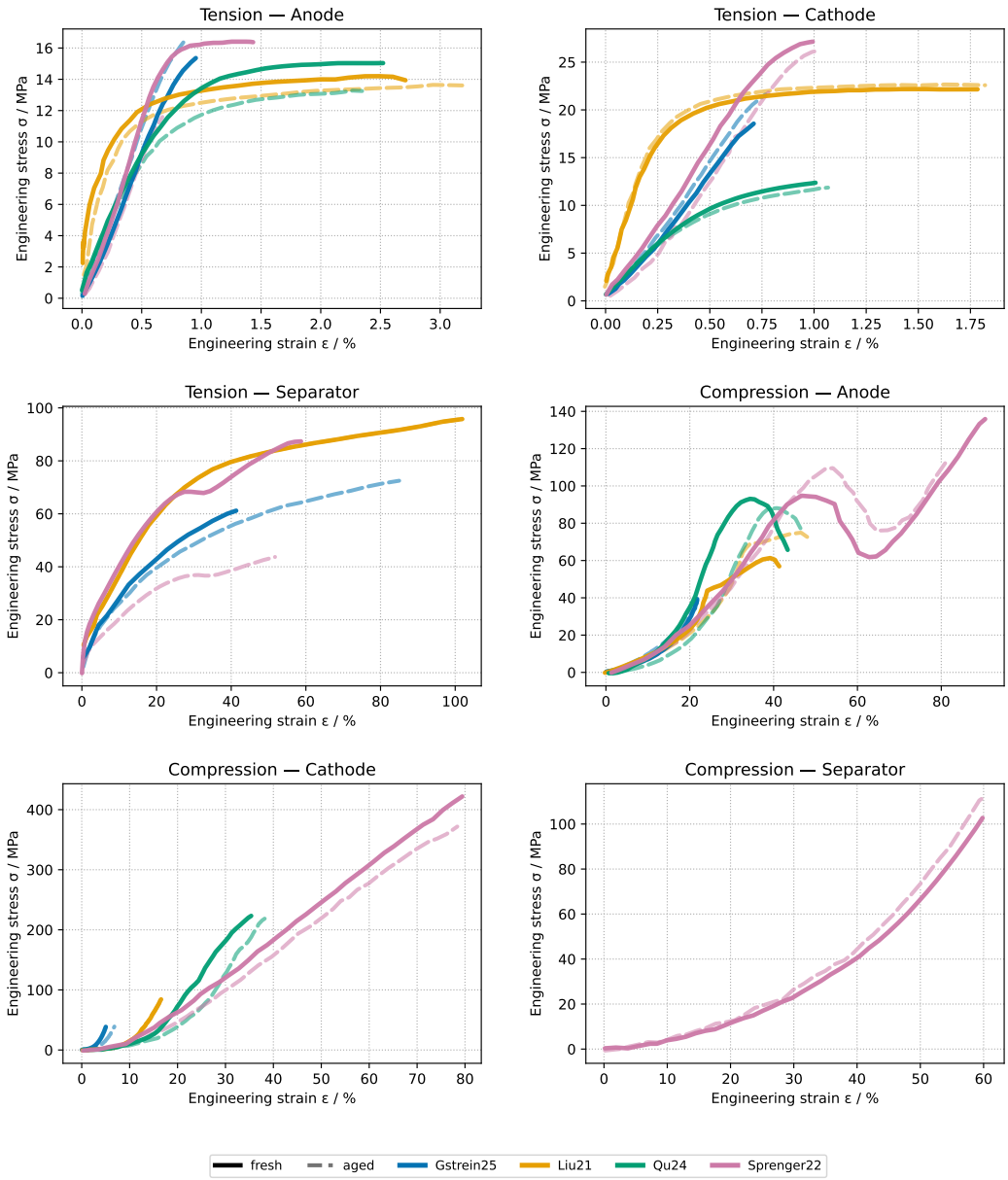

Figure 9. Cross-study engineering stress–strain responses of fresh and aged electrode and separator specimens. Force–displacement data were converted using the reported specimen geometries.

Taken together, these component-level observations support the view that aging can modify constituent properties such as strength, ductility, and compaction response in ways that may influence the macroscopic intrusion behavior of the cell. However, the direction of change is not consistent across studies, even though all were conducted on pouch cells, and the observed responses depend strongly on strain range and test boundary conditions. Component-level shifts therefore remain a plausibility layer and not a clear explanation of the compiled cell-level ratios.

When interpreted alongside the cell-level ratios, the component data suggest a plausible reason why force and displacement markers need not shift in the same direction

with aging. Aging-induced softening of the electrode stack, as indicated in several anode datasets and in some separator measurements, would tend to increase compliance and can therefore be consistent with larger intrusion at a bulk-mechanical marker such as peak force ($r_\delta > 1$). In contrast, degradation that lowers separator stiffness, strength, or puncture resistance could promote earlier local electrical contact and shift an ISC-based marker to smaller intrusion ($r_\delta < 1$). Thus, an aged cell may appear mechanically more compliant at the stack scale while also becoming more vulnerable to local short-circuit initiation. This distinction provides a physically plausible explanation for the observed decoupling of r_F and r_δ in Section 5.3, but it should be read as an interpretive framework rather than as a demonstrated mechanism.

The available component evidence does not yet allow this interpretation to be tested directly. The compiled stress–strain datasets stem exclusively from pouch-cell components, and differences in strain range, loading mode, extraction procedure, and aging protocol remain substantial. Evidence from hard-cased or cylindrical cells, such as Zhang et al. [17], is valuable because it points to separator degradation under a different architectural constraint, but it is not directly equivalent to the pouch-derived uniaxial tension and compression data shown in Figure 9. Consequently, the format-associated pattern observed at cell level cannot yet be assigned uniquely to intrinsic material aging, initial-thickness growth (Section 5.2), preserved casing constraint, or the confinement-history effects discussed in Section 5.4.1. Closing this gap would require matched fresh–aged extracted-component data from pouch and cylindrical or hard-cased cells aged under comparable protocols and tested under comparable mechanical modes.

At present, quantitative attribution of the compiled cell-level shifts to specific internal mediators remains unreliable because the available studies differ simultaneously in confinement conditions during aging and abuse, in the reported cell state at the time of intrusion (e.g., SoC, SoH, swelling-related preconditioning, or plating-related heterogeneity), and in the criteria used to define the reported marker. Current evidence therefore supports comparison of macro-scale shifts in reported force and displacement, but not unique assignment of these shifts to specific internal causal pathways. More fundamentally, mechanical failure progression diagnosis, that is, resolving how failure mechanically initiates and progresses as internal damage through the layered architecture, is still absent for the reported fresh-versus-aged abuse studies.

6. Electro-Thermal Response After the Declared Event

Section 5 examined whether aging shifts the reported mechanical event to earlier or later force–displacement states. The current question differs: after the electrically detected event is declared, does the subsequent response become milder or more severe? In intrusion and calorimetric safety studies, electrical collapse, temperature rise, venting, and TR are distinct but interrelated stages rather than a single synchronous event. Metrics such as voltage decay, temperature rise, heating rate, venting onset, and $T_{\max}$ therefore provide non-interchangeable information [26,78]. The post-event response is consequently interpreted from combined electrical and thermal signatures rather than from one scalar severity metric.

The integrated severity class is assigned by an explicit rule operating on three separately evaluated evidence domains: the electrical domain (voltage-collapse depth, recovery behavior, decay rate, and duration), the thermal domain (heating rate, temperature rise, $T_{\max}$, and integrated thermal exposure), and the gross-hazard domain (venting, fire, ejection, and TR occurrence). The rule is applied in a fixed order so that every case falls into exactly one class. A domain counts as resolved if its aging-related direction is reported, which includes the case of no measurable difference (counted as resolved but neither worsening nor improving). A domain whose sub-indicators point in opposing directions is

treated as mixed-within-domain and counts as resolved but neither worsening nor improving. Cases with fewer than two resolved domains are classified as insufficient evidence. Among the remaining cases, a case is classified as more severe if at least two domains worsen and none improves, and as less severe if at least two domains improve and none worsens. All other cases—including opposing domain trends, mixed-within-domain evidence, SoC or aging-state dependence, and cases in which only a single domain resolves to a direction—are classified as mixed/state-dependent. Applying this rule, the dynamic comparisons of Sprenger et al. [64], for which only the electrical domain is resolved, are classified as insufficient evidence instead of a nominal increased severity. The quasi-static SoC= 0% comparison of Sprenger et al. [70], in which the electrical domain worsens while the thermal domain is mixed-within-domain and the gross-hazard domain shows no TR in either state, has only one directional domain and is therefore classified as mixed/state-dependent. Kovachev et al. [67] remain classifiable through the resolved thermal and gross-hazard domains despite unresolved electrical detail. The resulting per-case classification is compiled in Table A4, and the electrical and thermal signatures on which it rests in Table A5.

Table 6 cross-tabulates the 22 comparisons by marker-shift and integrated severity class. Each marker-shift class contains more than one severity outcome; hence, no monotonic marker-to-severity relation is supported.

Table 6. Marker-shift class versus integrated post-event severity for the 22 fresh-to-aged comparisons.

Integrated Severity	Larger-Margin	Mixed	Lower-Margin	Total
More severe ↑	2	4	2	8
Mixed/state-dep. ↔	0	3	4	7
Less severe ↓	2	2	1	5
Insufficient evidence ∅	1	1	0	2
Total	5	10	7	22

Notes: ↑ = more severe after aging; ↔ = mixed or state-dependent response; ↓ = less severe after aging; and ∅ = insufficient evidence.

Three features follow. First, the direction of aging-related change cannot be inferred from a single observable such as T_{max}, TR occurrence, or voltage-drop depth alone. Second, a later reported mechanical marker does not imply a milder post-event response, nor does an earlier marker imply a more severe one. Third, because trigger definitions and post-event observability differ across studies, the comparison must remain directional and categorical rather than metric.

A first group of studies indicates reduced post-event severity after aging. Kovachev et al. [67] reported later failure together with a less violent TR process and lower ignition frequency in high-temperature-aged pouch cells. Qu et al. [68] similarly observed weaker electrical collapse and lower, later thermal maxima in room-temperature-aged pouch cells. Jia et al. [24] further showed that cycling can shift the response toward recoverable minor-ISC behavior with only limited heating. These cases suggest that some aging pathways can soften the short-circuit response or reduce the exothermic contribution after shorting.

A second group shows the opposite pattern. Liu et al. [65,66] found that low-temperature aging can increase voltage-collapse severity, accelerate delayed decay, intensify heating, and under dynamic loading produce TR at the lowest SoH. Guo et al. [73] reported loss of partial voltage rebounds and substantially higher local heating after overcharge aging. Sprenger et al. [70] found stronger voltage drop, faster initial heating, higher T_{max}, and higher fire affinity at high SoC. Polzer et al. [29] further show that severity may in-

crease through longer thermal exposure and more critical venting direction even when T_{max} changes only weakly. These studies demonstrate that aging can change not only when the reported event occurs, but also how the short-circuit pathway develops after declaration.

A third group remains mixed or state-dependent. Xu et al. [74] showed that post-event thermal response can change in opposite directions depending on SoC and chemistry. Spettmann et al. [69] found that aged cylindrical cells show altered soft-to-hard short progression without a clear monotonic thermal worsening. Gstrein et al. [71] and Abbas et al. [72] show that charged and discharged states can lead to different severity interpretations within otherwise related datasets. These cases reinforce that capacity-based SoH alone is not sufficient to predict post-event severity.

Although nail penetration lies outside the indentation and crush scope of the compiled ratio tables, adjacent penetration literature supports the same mechanism dependence. For 18,650 cells cycled at low temperature, Friesen et al. [79] observed intensified exothermic response and loss of the fresh-cell SoC dependence after aging. Paired studies further show that cells dominated by lithium plating and cells dominated by SEI growth can show different relations between trigger sensitivity and subsequent heat release [25,26]. These observations support the conclusion that the dominant aging mechanism, not only capacity-based SoH, co-determines post-trigger severity.

Figure 10 resolves the aggregate counts by source and additionally shows SoC, cell format, loading mode, and event-evidence tier.

Figure 10. Evidence map linking marker-shift class to integrated post-event severity. Circles and triangles denote cylindrical and pouch cells, respectively; filled and hollow markers denote quasi-static and dynamic loading; and orange, blue, and black marker edges denote evidence tiers E1, E2, and E3. Red and green background fields highlight the unfavorable lower-margin/more-severe and favorable larger-margin/less-severe combinations, respectively; pale-yellow fields denote the remaining classifiable combinations, and the gray field denotes insufficient evidence. Parenthetical values indicate test SoC.

The case-level distribution confirms that similar marker shifts can precede substantially different post-event trajectories.

7. From Macro-Scale Shifts to Crash-Relevant Interpretation: Diagnostics, Modeling, and Reporting Gaps

Section 5 demonstrates that the mechanically available margin to a study-defined declared event can shift with aging in either direction. Section 6 reveals that post-event outcomes remain heterogeneous despite nominally similar triggers. These findings collectively restrict direct inference from aged-versus-fresh onset shifts to crash-relevant safety conclusions. This section addresses the resulting interpretative gaps and outlines priorities for future datasets, including aging-aware validation targets, progression-resolved diagnostics, enhanced hazard contextualization, and more consistent study design and reporting.

7.1. The Modeling Gap: From BoL-Calibrated Toolchains to Aging-Aware Validation Targets

Current mechanical-abuse models for LIBs include layer-resolved formulations with numerous internal contacts [80], homogenized jellyroll descriptions [81], and reduced-order or surrogate approaches [82]. However, their predictive transfer is limited by two inputs that are rarely portable across studies: constitutive descriptions representing the tested cell state and internal contact logic governing load transfer, localization, and electrically sustained short-circuit formation. Even at BoL, coupled mechanical-electrical-thermal simulations rely on assumptions about friction, electrical contact, and separator failure that standard abuse tests do not uniquely constrain [83,84].

This limitation is evident in BoL studies. Wang et al. demonstrated that short-circuit criteria calibrated under several quasi-static loading conditions did not transfer uniformly. The strain-based criterion failed to reproduce minor shorts in bending, and dynamic loading altered ISC onset compared to quasi-static conditions [85]. For aged cells, this transfer issue intensifies because aging modifies the mechanical state these models aim to represent, including thickness evolution, residual stress development, and cohesion loss, while appropriate validation targets remain limited [68]. Consequently, many plausible workflows continue to extrapolate from BoL-based assumptions.

The primary gap lies not in model complexity but in validation against a clearly documented state and boundary-condition history. Aging-aware studies must provide paired observables linking the tested cell state, including confinement and pressure history, to the measured abuse response under matched external constraints. Without this continuity, simulations may reproduce responses while conflating intrinsic aging effects with fixture-dependent artifacts.

A minimum validation workflow, derived from the evidence in Section 5, should include four elements: (i) state-specific material updates from paired fresh and aged component measurements, (ii) consistent geometry, indenter definition, contact topology, and external constraint logic between fresh and aged model variants, (iii) initial validation against the measured shift in the study-specific marker under matched fresh-to-aged abuse conditions, and (iv) secondary validation using localization evidence from imaging or post mortem analysis when available. Although this approach does not eliminate uncertainty, it distinguishes measured constituent changes from remaining model-form uncertainty, thereby enhancing the interpretability of fresh-to-aged comparisons.

7.2. The Diagnostic Gap: Resolving Internal Deformation Pathways in Aged Cells

A significant limitation in the current literature is the absence of mechanism-resolved evidence for aged cells subjected to mechanical abuse. As discussed in Section 5, ISC onset is typically defined by an operational electrical criterion, while force inflections, stiffness

changes, or peak loads do not correspond uniquely to a single internal failure mechanism. Consequently, global observables such as force–displacement, voltage, and surface temperature remain necessary but insufficient, particularly when aging induces spatially heterogeneous degradation states [6].

For fresh cells, studies such as [3,53] illustrate the type of progression-resolved evidence needed to close this gap for aged cells. Their results show that localized diagnostic techniques are required to align electrical signatures with specific internal deformation and failure pathways, rather than inferring mechanism solely from global force–displacement or voltage responses. Relevant approaches include in situ X-ray methods, radiography, micro-CT, and state-preserving post mortem analysis. Comparable evidence for aged cells is considerably sparser within the reviewed mechanical-abuse literature. Most studies remain confined to macro observables, and only a few combine these with spatially resolved diagnostics under controlled preconditioning. Consequently, the physical interpretation of an earlier or later aged-cell trigger remains insufficiently resolved.

Available imaging evidence further shows that similar global force–displacement responses can arise from different internal deformation pathways and that onset markers may occur away from the point of maximum indentation depending on confinement and winding architecture [11]. For aged cells, an earlier or later ISC declaration may therefore reflect localized shear, distributed buckling, contact redistribution, or another concealed pathway. Aging-aware intrusion studies should therefore incorporate at least one localization method—preferably in situ, alternatively interruption with carefully documented post mortem mapping—that can be aligned with the reported trigger criterion. Only then can macro-scale onset shifts be interpreted as physically specific rather than purely operational differences.

7.3. The Coupled Hazards Gap: Contextualizing Post-Event Severity Beyond Mechanical Triggers

Section 6 demonstrates that post-event severity cannot be represented by a single scalar metric. In quasi-static indentation, ISC onset is typically detected by a voltage drop, while escalation is monitored through temperature increase, venting, or TR. Consequently, a voltage-drop-based trigger does not determine the subsequent thermal trajectory, which varies from limited heating to full thermal runaway depending on protocols and operating conditions [86]. Therefore, in crash-relevant assessments, the timing of the trigger point should not be considered a direct indicator of final hazard severity.

Aging further complicates this interpretation by altering the electro-thermal baseline from which mechanically induced faults develop. Thermal-abuse studies indicate that cycling history, storage conditions, and temperature exposure can shift TR onset temperatures and heat-release profiles even at comparable capacity-based SoH [87,88]. In mechanically abused aged pouch cells, aging correlates with modified force-displacement behavior and accelerated post-event voltage collapse and temperature increase [65]. Moreover, lithium plating and its relaxation history can significantly reduce exothermic onset temperatures and affect runaway severity under quasi-adiabatic conditions [89]. These results emphasize a key limitation identified throughout this review: when aging alters the fault evolution pathway, fresh high-SoC tests become less reliable proxies for the most critical adverse conditions.

Therefore, post-event outcomes should be reported and interpreted alongside explicit definitions of the mechanical and electrical markers, synchronized electro-thermal measurements, and a minimal set of state descriptors. While the mechanical trigger remains a critical reference point, it should not be considered the final determinant in safety interpretation. A key implication for future research is that hazard escalation must be regarded as a coupled response influenced by cell state, the relation between mechanical and electrical markers, and post-marker observability.

7.4. The Prediction Gap: Data-Driven and Digital Models of Aged-Cell Intrusion Safety

Beyond the finite-element toolchains discussed in Section 7.1, data-driven and hybrid approaches are increasingly proposed for battery safety. Physics-informed models combine simulation with measurements to estimate cell state and accelerate safety-relevant predictions [90], while multiphysics-coupled machine learning has been applied to thermal-runaway prediction at module level [91]. For aged-cell intrusion, the most relevant extension would link diagnosed aging state and mechanical boundary conditions to probabilistic short-circuit and hazard predictions. Such models could integrate impedance, swelling, imaging, force, voltage, and temperature data, but should complement rather than replace mechanically validated models.

The present synthesis clarifies why such models are not yet reliable for aged cells. Data-driven predictions become trustworthy only when the marker definition, the boundary-condition and confinement history, and the evidence strength behind a declared event are standardized. Otherwise a model trained on heterogeneously labeled data inherits precisely the confounds documented throughout this review, and the current training base is both small and inconsistently annotated. The three-tier framework and reporting checklist proposed here therefore define the metadata space that a credible data-driven or digital-twin model of aged-cell intrusion safety would require as input, and standardized labeling is a prerequisite for, rather than a consequence of, such models.

7.5. A Practical Roadmap for Future Study Design

A frequent source of over-interpretation in the literature is the discontinuity between the state established during aging and the state tested under abuse. This issue is especially critical for pouch cells, where stack pressure or module-like preload may exist during aging but is released prior to intrusion testing [65]. If this transition is not explicitly controlled and documented, observed aging or format effects may partially reflect boundary-condition history instead of intrinsic cell-state differences.

A minimum aging-aware reporting set must document the confinement conditions during both aging and abuse, the fixture concept used to maintain or release preload, the mechanical marker used for comparison, the electrical marker used to identify ISC-related response, and the time window used for post-marker severity classification. These variables are essential as they define the interpretive boundaries of the reported fresh-to-aged comparison. Table 7 operationalizes this requirement as a concrete, tier-resolved checklist that maps directly onto the three-tier framework of Figure 1. Each item is stated together with the quantity or unit that makes it cross-study comparable. Where the reviewed literature already contains an exemplary practice, it is cited as a template rather than as a prescription.

Beyond reporting, two deliberate study pairings would significantly enhance interpretability. First, matched versus released confinement should be explicitly compared when pouch-cell state continuity is uncertain. For pouch cells aged under sustained external compression, a preload-retaining setup is a strong candidate for the most internally consistent reference condition, but this expectation is currently supported only by fresh-cell evidence [51]. A controlled aged-cell comparison of retained versus released preload has not yet been reported and would directly quantify the confinement contribution discussed in Section 5.4.1, as well as the residual thickness contribution identified in Section 5.2. Second, macro-level trigger metrics should be paired with at least one localization observable that anchors the internal deformation pathway [92]. These pairings collectively facilitate the separation of intrinsic aging effects from fixture artifacts and ambiguity in the relation between reported electrical and mechanical markers.

For qualification practice, the immediate implication is not to replace BoL testing universally, but to supplement it with targeted aging-aware verification cases whenever service-induced state changes may alter the intrusion-to-hazard pathway. At the same time, comparisons between laboratory-aged and field-aged cells require careful qualification, because field use introduces additional and often poorly documented history variables. Two further aspects sharpen this requirement. First, the coupling between mechanical state and aging is bidirectional: even minor mechanical deformation that does not trigger an ISC has been shown to accelerate capacity fade and increase the thermal response of 18,650 cells during subsequent cycling, plausibly through localized lithium deposition [93]. Field-aged cells may therefore carry undocumented mechanical preconditioning that laboratory aging protocols do not reproduce. Second, safety assessments of nominally comparable aged cells diverge depending on whether lithium plating or SEI growth dominates the degradation, as demonstrated by the paired testing-method studies of Gerosa et al. [25] and Preger et al. [26]. Reporting the dominant aging mechanism, not only the capacity-based SoH, should therefore be part of the minimum aging-aware reporting set. The available evidence remains too discontinuous to support broad format-level conclusions without such qualification: field-aged pouch cells in [71,72] do not follow a simple pattern in which more aging produces a higher margin, whereas pronounced right-shifts were reported under specific laboratory protocols in [64,70]. Four next steps are therefore most urgent. The first is transparent reporting of confinement logic, trigger definitions, and monitoring windows across aging and abuse. The second is the generation of progression-resolved aged-cell datasets linking macro-scale shifts to internal deformation pathways [11,12,94]. The third and fourth are paired, event-resolved intrusion-abuse studies on aged LFP and prismatic cells: first mechanical characterizations of aged prismatic LFP cells now exist [77], but they do not report the paired fresh-to-aged force, displacement, and thickness data at a declared event that a normalized comparison requires. These priorities would most directly convert macro-scale observations into physically grounded and transferable safety conclusions.

Table 7. Minimum aging-aware reporting checklist for indentation and crush studies.

Tier	Item to Report	Comparable Quantity/Unit (Exemplary Practice)
1. Boundary conditions	Indenter geometry and size	Type + characteristic dimension (e.g., hemisphere ∅ 50 mm or rod ∅ 30 mm)
	Confinement during both aging and abuse	Preload pressure in MPa or "free", fixture concept, and whether preload is retained or released between phases [51]
	Loading mode and rate	QS in mm/min or dynamic in m/s, reporting the actual value and not only "quasi-static"
	SoC at abuse and cell format/chemistry	SoC in %, cell format, and cathode/anode chemistry
	Abuse temperature	Cell/ambient temperature in °C
2. Comparison-event declaration	Mechanical marker definition	State explicitly: peak force, first force drop, or inflection ($dF/d\delta$ maximum)
	Electrical ISC criterion	Threshold and evaluation window (e.g., net $\Delta V \leq -50$ mV within a sliding 0.10 s window [29])
	Paired fresh and aged values	Absolute $F_{fresh}, F_{aged}, \delta_{fresh}, \delta_{aged}$ and the derived r_F, r_δ
3. Post-event hazard	Synchronized channels	Time-aligned voltage and temperature (and, if possible, venting/imaging)
	Observation window/stop criterion	Duration in s after the declared marker and explicit stop rule
	Severity metrics (multiple)	Voltage-collapse depth, heating rate, T_{max}, integrated thermal exposure (K s), venting path, and TR (yes/no)
	Dominant aging mechanism	Li plating, SEI growth, or overcharge, not only capacity-based SoH [25,26]

7.6. Possible Recommendations for Standards and Lifetime Testing Programs

The comparability limitations documented in Section 3 suggest preliminary additions to abuse-testing standards and lifetime qualification programs. That standards are already

moving toward stricter and more state-aware criteria is illustrated by the revision of the Chinese national standard GB 38031: the 2025 edition, published on 28 March 2025 and in force from 1 July 2026, tightens the thermal-propagation test requirement from a warning issued before fire or explosion (2020 edition) to a "no fire, no explosion" criterion while retaining a warning obligation [46,95]. The following are therefore offered as possible recommendations, each following directly from a gap identified in this review:

1. Retain BoL testing as the reference condition, but supplement it risk-based with aged-cell verification whenever service-induced state changes may alter the intrusion-to-hazard pathway.
2. Define the aged state not only through capacity-based SoH but also through the dominant degradation mechanism, since safety assessments diverge between lithium-plating- and SEI-dominated aging at comparable SoH [25,26].
3. Document, and where possible preserve, the confinement conditions during both aging and abuse, and record whether preload is retained or released between the two phases.
4. Report the mechanical marker, the electrical event criterion, and the evidence supporting an ISC attribution as three separate items rather than as a single declared failure.
5. Require synchronized force, displacement, voltage, and temperature acquisition, with an explicit electrical criterion (e.g. a defined voltage-drop threshold and evaluation window [29]).
6. Standardize and report the post-event observation window and stop criterion, so that severity statements refer to a comparable time base.
7. Record cell thickness or irreversible swelling before the abuse test, enabling thickness-normalized displacement comparison (Section 5.2).
8. In lifetime programs, store mechanical preconditioning and module preload as explicit history variables, since even non-triggering deformation can accelerate subsequent degradation [93].
9. Make raw traces or standardized summary metrics available, so that future studies can be pooled quantitatively rather than only compared descriptively.

These items map onto the reporting checklist of Table 7 and are intended to make aging an explicit, documented variable in qualification rather than an unquantified source of divergence.

7.7. Synthesis of Open Scientific Problems

The gaps identified across this review are consolidated in Table 8, which states, for each open problem, why it remains unresolved, the minimal study design that would address it, and the expected benefit. The table states the minimum study design needed to address each open problem with currently available experimental methods.

Table 8. Priority research gaps and minimum study designs for aged-cell intrusion safety.

Open Problem	Why It Remains Unresolved	Minimal Study Design	Expected Benefit
Thickness-normalized intrusion (Section 5.2)	Displacement is referenced to first contact, so aging-induced swelling can inflate the nominal displacement-based intrusion margin	Report h_{fresh} and h_{aged} and evaluate δ/h alongside absolute travel	Robust displacement comparison that separates geometry from tolerance
Confinement continuity (Section 5.4.1)	No aged-cell study isolates retained versus released preload under otherwise identical conditions	Paired retained- vs. released-preload intrusion on the same aged cells	Separation of cell state from fixture artifact

Table 8. *Cont.*

Open Problem	Why It Remains Unresolved	Minimal Study Design	Expected Benefit
Event attribution (Section 2.1)	A voltage drop need not indicate internal electrode contact (tab, terminal, or measurement artifacts)	Synchronized voltage, force, and temperature with post-test imaging or a defined electrical criterion	Confirmed, evidence-graded fault attribution (E1–E3)
Severity classification (Section 6)	Severity is judged from inconsistent and incompletely resolved metrics	Predefined multi-domain rubric (≥2 resolved of electrical/thermal/gross-hazard)	Comparable, reproducible hazard statements
Under-represented technologies (Section 5.1)	Paired aged intrusion data are confined to pouch and cylindrical liquid-electrolyte cells	Aged LFP, prismatic, silicon-rich, and (where feasible) solid-state intrusion campaigns	Transferability of the framework beyond graphite/NMC
Data-driven prediction (Section 7.4)	Training data are small and heterogeneously labeled	Shared metadata schema with uncertainty quantification across formats and aging routes	Reliable probabilistic models and digital twins

8. Conclusions and Outlook

Indentation and crush tests remain essential crash-relevant surrogates for studying failure processes in mechanically intruded LIBs. Once aged cells are considered, however, the main challenge is no longer only whether a reported trigger occurs at smaller or larger intrusion. Interpretation also requires separating three distinct questions: under which boundary conditions damage develops, which study-specific mechanical and electrical markers are used to declare the event of interest, and how the electro-thermal response evolves after that declaration. Many apparent contradictions in the literature arise because these layers are not equivalent across studies and are not always reported with sufficient clarity. The primary contribution of this review is therefore not a new empirical trend but an operational framework (Figure 1) that separates these three layers and a concrete, tier-resolved reporting checklist (Table 7) that makes fresh-to-aged intrusion studies mutually comparable.

Three main conclusions emerge from the reviewed evidence. First, aging does not induce a universal directional shift in the mechanically available margin to a declared event. Depending on cell format, SoC, loading rate, temperature, aging route, and external constraint, the reported marker may shift toward either earlier or later force–displacement states. Neither reduced nor increased intrusion tolerance should therefore be interpreted as a general signature of aging. The descriptive synthesis quantifies this heterogeneity: force and displacement at the reported marker shift in the same direction in only 12 of 21 evaluable comparisons (14 of 21 after thickness normalization). The apparent pouch-cell right shift is also substantially attenuated once aging-induced growth of the initial thickness is accounted for, reducing the pouch median from $r_\delta = 1.07$ to $r_\varepsilon \approx 1.00$. The remaining variation differs across aging routes and test SoC conditions, but their individual contributions cannot be separated in the available dataset. Second, shifts in the reported mechanical or electrical marker cannot be mapped directly onto post-event hazard severity. An earlier declared trigger does not necessarily imply a stronger thermal escalation, and a later marker does not guarantee a milder outcome. The subsequent response depends on the declaration logic, the evidence strength behind the declared event, the observability window, the electro-thermal baseline of the cell, and the descriptors used to classify severity. Third, confinement continuity is an important interpretive variable, particularly for pouch cells. When cells are aged under stack pressure or module-like preload but tested later in a mechanically relaxed state, the structural condition established during aging is not preserved. Such discontinuity may alter the apparent abuse response and may

bias fresh-to-aged comparisons with hard-cased formats, where the external constraint is typically retained more consistently. Because no aged-cell study has yet compared retained against released preload under otherwise identical conditions, this discontinuity remains a candidate mediator rather than a demonstrated cause, and paired preload-retaining and preload-released intrusion tests on aged pouch cells are the single most informative experiment this review identifies.

At the same time, the current evidence base remains too limited for broad generalization. Aged intrusion datasets are still sparse for LFP and prismatic cells, and progression-resolved observations during intrusion are much less developed for aged cells than for fresh references. Cross-study comparability is further weakened by inconsistent trigger definitions, non-equivalent mechanical markers, and uneven post-marker monitoring. These limitations constrain both mechanistic interpretation and predictive model validation. Within this context, component-level fresh-to-aged measurements are most valuable when they are used as state-specific inputs or validation targets under matched cell-level boundary conditions, rather than as standalone explanations for macro-scale shifts.

The practical implication is that qualification strategies focused mainly on high-SoC cells at BoL remain important, but they cannot be assumed to bound intrusion sensitivity or post-event hazard severity throughout service life. The most sensible next steps are the generation of aged datasets for underrepresented formats and chemistries, especially LFP and prismatic cells, paired fresh-to-aged campaigns under rigorously fixed and explicitly reported confinement conditions, progression-resolved diagnostics aligned with the declared trigger logic, and aging-aware model validation that preserves continuity of state and boundary conditions. Adopting the tier-resolved reporting checklist proposed here (Table 7) is a low-cost first step that would let future studies be pooled quantitatively rather than only compared descriptively. Addressing these areas is essential before the intrusion response of aged cells can be translated into a mechanism-resolved and physics-based framework for crash-safety assessment and future certification logic.

Supplementary Materials: The following supporting information can be downloaded at https://www.mdpi.com/article/10.3390/batteries12080282/s1, File S1: The compiled per-comparison fresh-to-aged data (one row per comparison), listing the reported force and displacement ratios, the declared-event evidence tier, the marker-shift class, the integrated post-event severity class, and, for the pouch entries, the initial-thickness values and the initial-thickness-normalized ratio r_ε (CSV format). File S2: The Python 3.13.12 script that reproduces the descriptive robustness summaries of Table A3 directly from File S1, without any duplicated data.

Author Contributions: Conceptualization, R.P.; methodology, R.P.; software, R.P.; validation, R.P. and C.A.R.J.; formal analysis, R.P.; investigation, R.P.; resources, R.P.; data curation, R.P.; writing—original draft preparation, R.P.; writing—review and editing, R.P., C.A.R.J., S.D. and H.-G.S.; visualization, R.P.; supervision, S.D. and H.-G.S.; project administration, R.P.; funding acquisition, R.P. All authors have read and agreed to the published version of the manuscript.

Funding: This research received no external funding. The article processing charge was funded by the Open Access Publication Fund of Technische Hochschule Ingolstadt and by the Federal Ministry of Research, Technology and Space (BMFTR) through the FH-Personal project PTT_THI (grant number 03FHP188).

Data Availability Statement: All underlying measurements were extracted from the cited publications. The compiled per-comparison ratio data and the descriptive evaluation script are openly available as Supplementary Material (Files S1 and S2) accompanying this article. The digitized component-level curves underlying Figure 9 are reproduced from the cited primary sources and are available from the corresponding author on reasonable request.

Acknowledgments: During the preparation of this work, the authors used Grammarly for Microsoft Edge (version 14.1134.0) and ChatGPT using GPT-5.5 (OpenAI) solely for language editing and improvements in readability. The authors reviewed and edited all outputs as needed and take full responsibility for the content of the publication.

Conflicts of Interest: The authors declare no conflicts of interest.

Abbreviations

BoL	Beginning of Life
RT	Room Temperature
QS	Quasi-Static
DYN	Dynamic
EIS	Electrochemical Impedance Spectroscopy
IP	Inflection Point
ISC	Internal Short Circuit
LFP	Lithium Iron Phosphate
LIB	Lithium-Ion Battery
LTO	Lithium Titanate
NCA	Nickel Cobalt Aluminum Oxide
NCMA	Nickel Cobalt Manganese Aluminum Oxide
NMC	Nickel Manganese Cobalt Oxide
LCO	Lithium Cobalt Oxide
SEI	Solid Electrolyte Interphase
SoC	State of Charge
SoH	State of Health
TR	Thermal Runaway

Appendix A

Table A1. Confinement conditions during aging and subsequent mechanical abuse tests.

Source	Cell	Aging Confinement/Preload	Abuse Confinement
Abbas [72]	Pouch, NMC, 64.4 Ah	Flat plates, $p = 0.0084$ MPa	Free
Gstrein [71]	Pouch, NMC, 64.6 Ah	In module (preload n.r.)	Free
Qu [68]	Pouch, LCO, 4.1 Ah	Flat plates, $p = 0.05$ MPa	Free
Spettmann [69]	Pouch, NMC, 25 Ah	Flat plates, $p = 0.05$ MPa	Free
Jia [24]	Pouch, NCMA, 3.2 Ah	Free	Free
Sprenger [64]	Pouch, NMC, 74 Ah	In module (preload n.r.)	Free
Liu [66]	Pouch, NMC, 25 Ah	Flat plates, $p = 0.05$ MPa	Free
Sprenger [70]	Pouch, NMC, 74 Ah	In module (preload n.r.)	Free
Liu [65]	Pouch, NMC, 25 Ah	Flat plates, $p = 0.05$ MPa	Free
Kovachev [67]	Pouch, NMC, 41 Ah	Flat plates, $p = 0.06$ MPa	Free

Appendix A.1. Initial Cell Thickness and Thickness-Normalized Displacement Ratios

Table A2. Reported initial pouch-cell thicknesses and thickness-normalized displacement ratios.

Source/Case	$h_{fresh} \rightarrow h_{aged}$	h_{aged}/h_{fresh}	Basis of Thickness Values	r_δ	r_ε
Liu [65]	7.50 → 8.06 mm	1.075	text, 0% SoC, SoH 70%	1.16	1.08
Liu [66]	7.50 → 8.06 mm	1.075	same cells as [65]	1.00	0.93
Kovachev [67]	7.74 → 8.29 mm	1.071	Table (3 cells, 8 points); SoC at measurement n.r.	1.38	1.29
Qu [68]	4.59 → 5.11 mm	1.113	text/figure, 0% SoC, 30% fade	1.23	1.10
Jia [24]	rel. +3%	1.030	reported relative change	1.14	1.11
Spettmann [69] (P)	≈7.5 → ≈8.2 mm	≈1.09	read from published figure	1.17	1.07
Sprenger [64,70], 0% SoC	11.70 → 12.46 mm	1.065	table, SoC-matched; displ. reference n.r.	1.07	1.00
Sprenger [64,70], 100% SoC	12.15 → 13.93 mm	1.147	table, SoC-matched; displ. reference n.r.	1.50/1.60	1.31/1.40
Gstrein [71]	rel. ≈+3%	1.030	reported relative swelling	0.86/0.85	0.83/0.82
Abbas [72], field, 0/100% SoC	11.25/11.75 → 11.78/12.05 mm	1.047/1.026	table, SoC-matched	0.85/0.91	0.81/0.89
Abbas [72], Li-pl., 0/100% SoC	11.25/11.75 → 12.27/12.73 mm	1.091/1.083	table, SoC-matched	1.07/1.00	0.98/0.92
Guo [73]	rel. +20.67%	1.207	reported relative change, 0% SoC	1.29	1.07

Notes: $r_\varepsilon = r_\delta/(h_{aged}/h_{fresh})$ according to Equation (1). The displacement reference is first contact unless marked n.r.; paired values are reported as 0%/100% SoC. The dynamic entries of [64] are normalized using the SoC-matched thickness measurements for the same cell type in [70]. For [67], the SoC of the thickness measurement is not reported; the resulting r_ε should therefore be interpreted as an upper-bound estimate.

Appendix A.2. Descriptive Robustness of the Compiled Ratios

Table A3. Robustness summaries for reported and thickness-normalized displacement ratios.

Subset	Studies	Comparisons	Median r_δ (Range)	Median r_ε (Range)
Pouch, all comparisons	11	17	1.07 (0.85–1.60)	1.00 (0.81–1.40)
Pouch, one value per publication	11	—	1.17 (0.85–1.38)	1.08 (0.83–1.29)
Pouch, peak-force markers only	7	11	1.07 (0.85–1.38)	0.98 (0.81–1.29)
Pouch, artificially cycled	9	12	1.15 (1.00–1.60)	1.08 (0.92–1.40)
Pouch, field-aged	2	4	0.86 (0.85–0.91)	0.83 (0.81–0.89)
Cylindrical, all comparisons	3	5	0.84 (0.74–0.98)	n.a.
Cylindrical, excl. present study	2	3	0.97 (0.74–0.98)	n.a.

Notes: Values are medians with ranges in parentheses. In the second row, each publication contributes one within-study median. The analysis is descriptive; no pooling, weighting, or significance testing was applied. r_ε is defined only for pouch cells. Files S1 and S2 contain the per-comparison data and evaluation script.

Appendix A.3. Source-Level Post-Event Classification

Table A4. Source-level post-event severity classification.

Source/Case	Marker Class	Electrical	Thermal	Gross Hazard	Integrated
Liu [65]	larger →	↑	↑	≈	more severe ↑
Liu [66]	mixed ↔	↑	↑	↑	more severe ↑
Kovachev [67]	larger →	?	↓	↓	less severe ↓
Qu [68]	larger →	↓	↓	≈	less severe ↓
Jia [24]	mixed ↔	↓	↓	↓	less severe ↓
Spettmann [69] (C)	lower ←	↔	↔	≈	mixed ↔

Table A4. *Cont.*

Source/Case	Marker Class	Electrical	Thermal	Gross Hazard	Integrated
Spettmann [69] (P)	larger →	↑	↑	≈	more severe ↑
Sprenger [70], 0% SoC	mixed ↔	↑	↔	≈	mixed ↔
Sprenger [70], 100% SoC	mixed ↔	↑	↑	↑	more severe ↑
Sprenger [64], 0% SoC	mixed ↔	↑	?	?	insufficient ∅
Sprenger [64], 100% SoC	larger →	↑	?	?	insufficient ∅
Gstrein [71]	lower ←	↔	↔	≈	mixed ↔
Abbas [72], Field, 0%	lower ←	↓	↓	≈	less severe ↓
Abbas [72], Field, 100%	lower ←	↔	↔	≈	mixed ↔
Abbas [72], Li-pl., 0%	mixed ↔	↓	↓	≈	less severe ↓
Abbas [72], Li-pl., 100%	mixed ↔	↑	↑	↑	more severe ↑
Guo [73]	mixed ↔	↑	↑	≈	more severe ↑
Xu [74]	mixed ↔	↔	↔	≈	mixed ↔
Polzer [29]	lower ←	↑	↑	↑	more severe ↑

Notes: Domain symbols: ↑ more severe with aging, ↓ less severe, ↔ mixed or opposing within the domain, ≈ resolved but no measurable aging difference (e.g., no TR in either state), ? not reported or not resolved. Integrated class (rule of Section 6): cases with fewer than two resolved domains are insufficient (∅); among the remaining cases, more severe if ≥2 domains worsen and none improves, less severe if ≥2 improve and none worsens, and mixed in every other case (opposing domain trends, mixed-within-domain evidence, state dependence, or only a single directional domain). Marker class (reported ratios, exact unity threshold): the right arrow (→) denotes the larger-margin class with $r_F > 1$ and $r_\delta > 1$, the left arrow (←) denotes the lower-margin class with $r_F < 1$ and $r_\delta < 1$, and the bidirectional arrow (↔) denotes every remaining mixed case (discordant or unity-valued marker shifts). Under the thickness normalization of Section 5.2, only the two Abbas Li-pl. entries change marker class (mixed to lower); all other assignments are normalization-invariant. Study-level rows for Gstrein, Xu, and Polzer each aggregate two SoC-resolved comparisons of the same class, so the 19 rows correspond to the 22 compiled comparisons.

Appendix A.4. Detailed Post-Event Response Signatures

Table A5. Detailed electrical and thermal post-event response signatures.

Source	Post-Event Response Signatures		Aging-Related Overall Trend
	Electrical Response	Thermal Response	
Liu [65]	Larger voltage drop during loading and earlier transition to rapid delayed decay with aging. At 30% fade, deep voltage drop with partial voltage recovery.	No TR. Higher temperatures at 10–20% fade and strongly localized center heating at 30% fade.	**Increased electro-thermal severity**: despite later mechanical failure, aging accelerates electrical discharge and intensifies, especially localizes, heating.
Liu [66]	Initial voltage drop with partial recovery during intrusion. Faster long-term voltage decay with aging.	Thermal response increases with aging. TR observed at 30% fade under dynamic loading.	**Increased electro-thermal severity**: aging strengthens the long-term electrical and thermal escalation, most clearly at low SoH under dynamic loading.
Kovachev [67]	Abrupt voltage collapse near peak load. Detailed post-event voltage subclasses are not reported.	TR in both states, but aged cells show less smoke and a less violent TR process. Only two of three aged cells ignite.	**Reduced electro-thermal severity**: aging is associated with a milder thermal reaction despite later failure.
Qu [68]	Smaller instantaneous voltage drop and longer time to 1 V when aged.	No TR. Lower T_{max} and later temperature peak with aging.	**Reduced electro-thermal severity**: aging is associated with weaker electrical collapse and slower, lower heating.

Table A5. *Cont.*

Source	Post-Event Response Signatures		Aging-Related Overall Trend
	Electrical Response	**Thermal Response**	
Jia [24]	Cycling increases the occurrence of recoverable voltage-response mode (Mode III) instead of sustained major short-circuit behavior.	Recoverable cases show only slight local heating. In non-recovered cases, temperature rise and heating rate decrease with cycling.	**Reduced electro-thermal severity**: aging shifts the response toward softer ISC modes and milder thermal evolution.
Spettmann [69] (Cyl.)	Soft short followed by hard short. The interval between both increases with aging.	No TR. T_{max} occurs later when aged, without a clear monotonic increase in severity.	**Mixed/no clear directional trend**: aging alters ISC progression, but a systematic increase in thermal severity is not established.
Spettmann [69] (Pouch)	Faster post-event voltage decay and shorter electrical energy-release duration when aged.	No TR. Higher temperatures across the pouch cell after aging.	**Increased electro-thermal severity**: aging accelerates electrical collapse and increases thermal response in pouch cells.
Sprenger [70]	Aged cells show stronger post-event voltage drop under cylindrical indentation.	At 100% SoC, aged cells show faster initial heating, higher T_{max}, and higher fire affinity. At 0% SoC, no TR occurs.	**State-dependent**: at 100% SoC the electrical, thermal, and gross-hazard domains all worsen (more severe); at 0% SoC only the electrical domain worsens while no TR occurs, so this case is classified as mixed.
Sprenger [64]	Steeper and deeper voltage collapse after failure under quasi-static and dynamic indentation.	Thermal response not directly resolved.	**Insufficient evidence**: only the electrical domain is resolved, so no severity direction is assigned under the domain rule of Section 6.
Gstrein [71]	Abrupt voltage collapse at failure. Aged charged cells show a deeper drop, whereas in discharged tests the larger drop is observed in fresh cells.	TR at 100% SoC for both fresh and aged cells. No relevant heating at discharged state.	**Mixed/state-dependent**: thermal escalation is primarily SoC-controlled, and the electrical trend is not directionally stable across states.
Abbas [72] 0% SoC	Aged and Li-plating-aged cells show a smaller and more gradual voltage drop than fresh cells. Slight pre-failure voltage rise is reported for Li-plating-aged cells.	No TR. The pouch remains intact and the response remains mild.	**Reduced electro-thermal severity**: at discharged state, aging does not intensify the post-event response and may soften the electrical collapse.
Abbas [72] 100% SoC	Li-plating-aged cells show the strongest voltage collapse. Partial voltage recovery may follow the initial drop during ongoing failure progression.	TR in all cases. Li-plating-aged cells are interpreted as more critical because of stronger electrical collapse and the reactivity of plated lithium.	**Increased electro-thermal severity**: for charged cells, Li-plating-induced aging intensifies the post-event response.
Guo [73]	Abrupt voltage collapse at peak force. Fresh cells show repeated partial voltage rebounds, whereas rebounds diminish with aging and disappear at SoH 70%.	No TR (tests at 10% SoC). Heating concentrated at the indentation site, with a sharp temperature spike and approximately 70% higher peak surface temperature at SoH 70% than for fresh cells.	**Increased electro-thermal severity**: overcharge cycling promotes harder, more localized short circuits with faster and stronger local heating despite the later mechanical marker.
Xu [74]	Early micro-short precedes fracture-induced major voltage collapse. Detailed post-event voltage subclasses are not reported.	No TR in the reported cases. Surface temperature rise changes with aging depending on SoC and chemistry.	**Mixed/SoC- and chemistry-dependent**: no single monotonic aging trend in post-event thermal severity is supported.
Polzer [29]	Fresh cells show more gradual voltage decline. Cells aged at 20 °C/20 A show abrupt collapse, whereas cells aged at −10 °C/45 A respond more heterogeneously.	TR in all groups. Peak temperatures remain broadly similar, but integrated temperature exposure increases with aging and venting shifts more often toward the top terminal.	**Increased electro-thermal severity**: aging prolongs external thermal exposure and makes venting direction more critical, even when T_{max} alone changes little.

Notes: "Electrical response" summarizes the dominant voltage evolution reported after ISC. "Thermal response" summarizes the reported heating behavior, including TR occurrence and, where available, intensity, timing, localization, or duration. "Aging-related overall trend" denotes the direction of the aged-versus-fresh shift within the respective study configuration, based jointly on the electrical and thermal response signatures. No single scalar severity metric is implied.

References

1. Cortada-Torbellino, M.; Elvira, D.G.; El Aroudi, A.; Valderrama-Blavi, H. Review of Lithium-Ion Battery Internal Changes Due to Mechanical Loading. *Batteries* **2024**, *10*, 258. [CrossRef]
2. Newaz, G.; Mundhe, S.; Arava, L.; Zhu, M.; Faruque, O.; Barbat, S. Direct Assessment of Separator Strain in Li-Ion Batteries at the Onset of Mechanically Induced Short Circuit. *Energies* **2020**, *13*, 669. [CrossRef]
3. Wang, H.; Simunovic, S.; Maleki, H.; Howard, J.N.; Hallmark, J.A. Internal configuration of prismatic lithium-ion cells at the onset of mechanically induced short circuit. *J. Power Sources* **2016**, *306*, 424–430. [CrossRef]
4. Long, T.; Wang, L.; Kan, C.D. Experimental and modeling approaches for electric vehicle battery safety: A technical review. *Eng. Res. Express* **2024**, *6*, 032503. [CrossRef]
5. Li, J.; Duan, X.; Li, B.; Chen, J.; Xie, S.; Wang, L. Revealing the internal short circuit mechanisms and progressive failure behaviors in electrodes of lithium-ion batteries upon dynamic loading. *J. Power Sources* **2025**, *652*, 237618. [CrossRef]
6. Zhu, X.; Wang, H.; Wang, X.; Gao, Y.; Allu, S.; Cakmak, E.; Wang, Z. Internal short circuit and failure mechanisms of lithium-ion pouch cells under mechanical indentation abuse conditions: An experimental study. *J. Power Sources* **2020**, *455*, 227939. [CrossRef]
7. Müller, V.; Scurtu, R.G.; Richter, K.; Waldmann, T.; Memm, M.; Danzer, M.A.; Wohlfahrt-Mehrens, M. Effects of Mechanical Compression on the Aging and the Expansion Behavior of Si/C-Composite | NMC811 in Different Lithium-Ion Battery Cell Formats. *J. Electrochem. Soc.* **2019**, *166*, A3796–A3805. [CrossRef]
8. Lian, J.; Wierzbicki, T.; Zhu, J.; Li, W. Prediction of shear crack formation of lithium-ion batteries under rod indentation: Comparison of seven failure criteria. *Eng. Fract. Mech.* **2019**, *217*, 106520. [CrossRef]
9. Zhu, J.; Li, W.; Wierzbicki, T.; Xia, Y.; Harding, J. Deformation and failure of lithium-ion batteries treated as a discrete layered structure. *Int. J. Plast.* **2019**, *121*, 293–311. [CrossRef]
10. Zhu, J.; Luo, H.; Li, W.; Gao, T.; Xia, Y.; Wierzbicki, T. Mechanism of strengthening of battery resistance under dynamic loading. *Int. J. Impact Eng.* **2019**, *131*, 78–84. [CrossRef]
11. Kisters, T.; Kuder, J.; Töpel, A.; Langkemper, R.; Nau, S.; Schopferer, S. Strain-rate dependence of the failure behavior of Lithium-Ion pouch cells under impact loading. *J. Energy Storage* **2021**, *41*, 102901. [CrossRef]
12. An, Z.; Shi, T.; Du, X.; An, X.; Zhang, D.; Bai, J. Experimental study on the internal short circuit and failure mechanism of lithium-ion batteries under mechanical abuse conditions. *J. Energy Storage* **2024**, *89*, 111819. [CrossRef]
13. Spielbauer, M.; Peteler, F.; Németh, A.; Soellner, J.; Berg, P.; Bohlen, O.; Jossen, A. An analysis of the current state and obstacles in discrete layered finite element simulation of crushing cylindrical lithium-ion cells. *J. Energy Storage* **2023**, *72*, 108029. [CrossRef]
14. Feiler, S.; Daubinger, P.; Gold, L.; Hartmann, S.; Giffin, G.A. Interplay between Elastic and Electrochemical Properties during Active Material Transitions and Aging of a Lithium–Ion Battery. *Batter. Supercaps* **2023**, *6*, e202200518. [CrossRef]
15. Jeon, D.H.; Kim, S.; Hempelmann, R. State-of-the-art review of degradation mechanisms of commercial lithium-ion batteries. *J. Power Sources* **2025**, *646*, 237242. [CrossRef]
16. Wang, Y.; Xiang, H.; Soo, Y.Y.; Fan, X. Aging mechanisms, prognostics and management for lithium-ion batteries: Recent advances. *Renew. Sustain. Energy Rev.* **2025**, *207*, 114915. [CrossRef]
17. Zhang, X.; Zhu, J.; Sahraei, E. Degradation of battery separators under charge–discharge cycles. *RSC Adv.* **2017**, *7*, 56099–56107. [CrossRef]
18. Blažek, P.; Klvač, O.; Šedina, M.; Čech, O.; Tkadlecová, M.; Stravová, Z.; Kazda, T.; Zikmund, T.; Schmitt, R.H.; Kaiser, J. Comprehensive analysis of degradation mechanisms in 18650 Li-Ion cells under prolonged cycling conditions. *J. Energy Storage* **2025**, *130*, 117436. [CrossRef]
19. Ralls, A.M.; Leong, K.; Clayton, J.; Fuelling, P.; Mercer, C.; Navarro, V.; Menezes, P.L. The Role of Lithium-Ion Batteries in the Growing Trend of Electric Vehicles. *Materials* **2023**, *16*, 6063. [CrossRef] [PubMed]
20. Ruiz, V.; Pfrang, A.; Kriston, A.; Omar, N.; van den Bossche, P.; Boon-Brett, L. A review of international abuse testing standards and regulations for lithium ion batteries in electric and hybrid electric vehicles. *Renew. Sustain. Energy Rev.* **2018**, *81*, 1427–1452. [CrossRef]
21. Sun, S.; Xu, J. Safety behaviors and degradation mechanisms of aged batteries: A review. *Energy Mater. Devices* **2024**, *2*, 9370048. [CrossRef]
22. Adebanjo, I.T.; Eko, J.; Agbeyegbe, A.G.; Yuk, S.F.; Cowart, S.V.; Nagelli, E.A.; Burpo, F.J.; Allen, J.L.; Tran, D.T.; Bhattarai, N.; et al. A comprehensive review of lithium-ion battery components degradation and operational considerations: A safety perspective. *Energy Adv.* **2025**, *4*, 820–877. [CrossRef]
23. Jaguemont, J.; Bardé, F. A critical review of lithium-ion battery safety testing and standards. *Appl. Therm. Eng.* **2023**, *231*, 121014. [CrossRef]
24. Jia, Y.; Gao, X.; Ma, L.; Xu, J. Comprehensive Battery Safety Risk Evaluation: Aged Cells versus Fresh Cells Upon Mechanical Abusive Loadings. *Adv. Energy Mater.* **2023**, *13*, 2300368. [CrossRef]

25. Gerosa, G.G.; Feinauer, M.; Hogrefe, C.; Häfele, S.; Bischof, K.; Wörz, M.; Böse, O.; Wohlfahrt-Mehrens, M.; Hölzle, M.; Waldmann, T. Impact of Testing Method on Safety Assessment of Aged Li-ion Cells: Part I—Li Plating as Main Aging Mechanism. *J. Electrochem. Soc.* **2025**, *172*, 030502. [CrossRef]
26. Preger, Y.; Feinauer, M.; Torres-Castro, L.; Hogrefe, C.; Gray, L.; Gerosa, G.; Langendorf, J.; Häfele, S.; Wittman, R.M.; Wörz, M.; et al. Impact of Testing Method on Safety Assessment of Aged Li-Ion Cells: Part II—Aged Cells Without Li Plating. *J. Electrochem. Soc.* **2025**, *172*, 080503. [CrossRef]
27. Awan, U.; Ghabraie, K.; Zolfagharian, A.; Rolfe, B. Impact of vibrations on lithium-ion batteries in electric vehicles: Sources, degradation mechanisms, and testing standards. *J. Phys. Energy* **2025**, *7*, 022003. [CrossRef]
28. Dini, P.; Colicelli, A.; Saponara, S. Review on Modeling and SOC/SOH Estimation of Batteries for Automotive Applications. *Batteries* **2024**, *10*, 34. [CrossRef]
29. Polzer, R.; Heider, E.; Ellersdorfer, C.; Golla-Schindler, U.; Rufino Júnior, C.A.; Diel, S.; Schweiger, H.G. Effect of Electrochemical Aging on the Mechanical–Electrical–Thermal Safety Response of Tabless 4695 Cylindrical Cells Under Quasi-Static Indentation. *Batteries* **2026**, *12*, 179. [CrossRef]
30. Lai, X.; Yao, J.; Jin, C.; Feng, X.; Wang, H.; Xu, C.; Zheng, Y. A Review of Lithium-Ion Battery Failure Hazards: Test Standards, Accident Analysis, and Safety Suggestions. *Batteries* **2022**, *8*, 248. [CrossRef]
31. *UN 38.3*; Recommendations on the Transport of Dangerous Goods—Manual of Tests and Criteria. United Nations: New York, NY, USA, 2015.
32. United Nations Economic Commission for Europe. *Global Technical Regulation No. 20: Electric Vehicle Safety (EVS)*; United Nations Economic Commission for Europe: Geneva, Switzerland, 2018.
33. United Nations Economic Commission for Europe. *UN Regulation No. 100, Revision 3: Uniform Provisions Concerning the Approval of Vehicles with Regard to Specific Requirements for the Electric Power Train*; United Nations Economic Commission for Europe: Geneva, Switzerland, 2022. Available online: https://unece.org/transport/documents/2022/03/standards/regulation-no-100-rev3 (accessed on 1 July 2026).
34. *ECE R136*; Regulation No. 136 of the Economic Commission for Europe of the United Nations (UN/ECE)—Uniform Provisions Concerning the Approval of Vehicles of Category L with Regard to Specific Requirements for the Electric Power Train. United Nations Economic Commission for Europe: Geneva, Switzerland, 2019.
35. *SAE J2380_202112*; Vibration Testing of Electric Vehicle Batteries. SAE International: Warrendale, PA, USA, 2021. https://doi.org/10.4271/J2380_202112.
36. *SAE J2464*; Electric and Hybrid Electric Vehicle Rechargeable Energy Storage System (RESS) Safety and Abuse Testing. Battery Safety Standards Committee: Warrendale, PA, USA, 2021.
37. *SAE J2929_201302*; Safety Standard for Electric and Hybrid Vehicle Propulsion Battery Systems Utilizing Lithium-Based Rechargeable Cells. SAE International: Warrendale, PA, USA, 2013. https://doi.org/10.4271/J2929_201302.
38. Doughty, D.H.; Crafts, C.C. *FreedomCAR Electrical Energy Storage System Abuse Test Manual for Electric and Hybrid Electric Vehicle Applications*; Sandia Report SAND2005-3123; Sandia National Laboratories: Albuquerque, NM, USA, 2006. https://doi.org/10.2172/889934.
39. *UL 2580*; Batteries for Use in Electric Vehicles, 3rd ed. UL Standards & Engagement: Northbrook, IL, USA, 2020; Revised 28 June 2022. Available online: https://www.shopulstandards.com/ProductDetail.aspx?productId=UL2580_3_S_20200311 (accessed on 1 July 2026).
40. United States Advanced Battery Consortium. *Electric Vehicle Battery Test Procedures Manual*; Revision 2; Report DOE/ID-10479; U.S. Department of Energy: Idaho Falls, ID, USA, 1996. Available online: https://www.osti.gov/biblio/214312 (accessed on 1 July 2026).
41. *IEC 62281*; Sicherheit von Primären und Sekundären Lithiumzellen und -Batterien beim Transport. International Electrotechnical Commission: Geneva, Switzerland, 2024.
42. *IEC 62660-2*; Lithium-Ionen-Sekundärzellen für den Antrieb von Elektrostraßenfahrzeugen, Teil 2: Zuverlässigkeits- und Missbrauchsprüfung. International Electrotechnical Commission: Geneva, Switzerland, 2020.
43. *IEC 62660-3:2022*; Secondary Lithium-Ion Cells for the Propulsion of Electric Road Vehicles—Part 3: Safety Requirements. International Electrotechnical Commission: Geneva, Switzerland, 2022.
44. *IEC 62133-2*; Sekundärzellen und -Batterien mit Alkalischen oder Anderen Nicht-säurehaltigen Elektrolyten—Sicherheitsanforderungen für tragbare Gasdichte Sekundärzellen und Daraus Hergestellte Batterien für die Verwendung in Tragbaren Geräten, Teil 2: Lithium-Systeme. International Electrotechnical Commission: Geneva, Switzerland, 2022.
45. *ISO 6469-1:2019*; Electrically Propelled Road Vehicles—Safety Specifications—Part 1: Rechargeable Energy Storage System (RESS). International Organization for Standardization: Geneva, Switzerland, 2019.
46. *GB 38031-2020*; Electric Vehicles Traction Battery Safety Requirements. State Administration for Market Regulation and Standardization Administration of China: Beijing, China, 2020.

47. *AIS-048*; Battery Operated Vehicles—Safety Requirements of Traction Batteries. Automotive Research Association of India: Pune, India, 2009.
48. Ministry of Land, Transport and Maritime Affairs, Republic of Korea. *KMVSS Article 18-3: Safety Requirements for Traction Batteries*; Ministry of Land, Transport and Maritime Affairs: Gwacheon, Republic of Korea, 2009.
49. Kotak, B.; Kotak, Y.; Brade, K.; Kubjatko, T.; Schweiger, H.G. Battery Crush Test Procedures in Standards and Regulation: Need for Augmentation and Harmonisation. *Batteries* **2021**, *7*, 63. [CrossRef]
50. Fasching, M.; Grollitsch, S.; Höschele, P.; Schmid, A.; Ellersdorfer, C. Investigating the mechanical in-plane characteristics of lithium-ion pouch cells under crush loads. *J. Energy Storage* **2024**, *89*, 111581. [CrossRef]
51. Höschele, P.; Heindl, S.F.; Erker, S.; Ellersdorfer, C. Influence of reversible swelling and preload force on the failure behavior of a lithium-ion pouch cell tested under realistic boundary conditions. *J. Energy Storage* **2023**, *65*, 107228. [CrossRef]
52. Wang, R.; Liu, G.; Wang, C.; Ji, Z.; Yu, Q. A comparative study on mechanical-electrical-thermal characteristics and failure mechanism of LFP/NMC/LTO batteries under mechanical abuse. *eTransportation* **2024**, *22*, 100359. [CrossRef]
53. Chung, S.H.; Tancogne-Dejean, T.; Zhu, J.; Luo, H.; Wierzbicki, T. Failure in lithium-ion batteries under transverse indentation loading. *J. Power Sources* **2018**, *389*, 148–159. [CrossRef]
54. Zhu, J. Standardizing mechanical tests on li-ion batteries to develop a useful cell-level model under extreme mechanical loads. *J. Energy Storage* **2023**, *65*, 107320. [CrossRef]
55. Dixon, B.; Mason, A.; Sahraei, E. Effects of electrolyte, loading rate and location of indentation on mechanical integrity of li-ion pouch cells. *J. Power Sources* **2018**, *396*, 412–420. [CrossRef]
56. Hartmann, L.; Reuter, L.; Wallisch, L.; Beiersdorfer, A.; Adam, A.; Goldbach, D.; Teufl, T.; Lamp, P.; Gasteiger, H.A.; Wandt, J. Depletion of Electrolyte Salt Upon Calendaric Aging of Lithium-Ion Batteries and its Effect on Cell Performance. *J. Electrochem. Soc.* **2024**, *171*, 060506. [CrossRef]
57. Kisters, T.; Sahraei, E.; Wierzbicki, T. Dynamic impact tests on lithium-ion cells. *Int. J. Impact Eng.* **2017**, *108*, 205–216. [CrossRef]
58. Wang, W.; Yang, S.; Lin, C.; Li, Y. State of Charge Dependent Constitutive Model of the Jellyroll of Cylindrical Lithium-Ion Cells. *IEEE Access* **2018**, *6*, 26358–26366. [CrossRef]
59. Deng, J.; Smith, I.; Bae, C.; Rairigh, P.; Miller, T.; Surampudi, B.; L'Eplattenier, P.; Caldichoury, I. Impact Modeling and Testing of Pouch and Prismatic Cells. *J. Electrochem. Soc.* **2020**, *167*, 090550. [CrossRef]
60. Kotter, P.; Kisters, T.; Schleicher, A. Dynamic impact tests to characterize the crashworthiness of large-format lithium-ion cells. *J. Energy Storage* **2019**, *26*, 100948. [CrossRef]
61. Zhang, X.c.; Zhang, T.; Liu, N.n.; Yin, X.d.; Wu, X.n.; Han, H.l.; Wang, Q.l.; Zhang, Y.j. Dynamic crushing behaviors and failure of cylindrical lithium-ion batteries subjected to impact loading. *Eng. Fail. Anal.* **2023**, *154*, 107653. [CrossRef]
62. Mo, F.; Tian, Y.; Zhao, S.; Xiao, Z.; Ma, Z. Working temperature effects on mechanical integrity of cylindrical lithium-ion batteries. *Eng. Fail. Anal.* **2022**, *137*, 106399. [CrossRef]
63. Gilaki, M.; Sahraei, E. Effects of Temperature on Mechanical Response of Lithium Ion Batteries to External Abusive Loads. In *Proceedings of the WCX SAE World Congress Experience, Detroit, MI, USA, 9 April 2019*; SAE Technical Paper Series; SAE International: Warrendale, PA, USA, 2019. [CrossRef]
64. Sprenger, M.; Kovachev, G.; Dölle, N.; Schauwecker, F.; Sinz, W.; Ellersdorfer, C. Changes in the Mechanical Behavior of Electrically Aged Lithium-Ion Pouch Cells: In-Plane and Out-of-Plane Indentation Loads with Varying Testing Velocity and State of Charge. *Batteries* **2023**, *9*, 67. [CrossRef]
65. Liu, Y.; Xia, Y.; Zhou, Q. Effect of low-temperature aging on the safety performance of lithium-ion pouch cells under mechanical abuse condition: A comprehensive experimental investigation. *Energy Storage Mater.* **2021**, *40*, 268–281. [CrossRef]
66. Liu, Y.; Xia, Y.; Xing, B.; Zhou, Q. Mechanical-electrical-thermal responses of lithium-ion pouch cells under dynamic loading: A comparative study between fresh cells and aged ones. *Int. J. Impact Eng.* **2022**, *166*, 104237. [CrossRef]
67. Kovachev, G.; Ellersdorfer, C.; Gstrein, G.; Hanzu, I.; Wilkening, H.M.R.; Werling, T.; Schauwecker, F.; Sinz, W. Safety assessment of electrically cycled cells at high temperatures under mechanical crush loads. *eTransportation* **2020**, *6*, 100087. [CrossRef]
68. Qu, Y.; Xing, B.; Xia, Y.; Zhou, Q. How does room temperature cycling ageing affect lithium-ion battery behaviors under extreme indentation? *eTransportation* **2024**, *20*, 100331. [CrossRef]
69. Spettmann, C.; Shin, J.; Qu, Y.; Liu, Y.; Xia, Y. Low-Temperature Aging Effect on Safety of Lithium-Ion Batteries Subjected to Intrusion: A Comparative Study of 18650 and Pouch Cells. In *Proceedings of the WCX SAE World Congress Experience, Detroit, MI, USA, 16 April 2024*; Spettmann, C., Shin, J., Qu, Y., Liu, Y., Xia, Y., Eds.; SAE Technical Paper Series; SAE International: Warrendale, PA, USA, 2024. [CrossRef]
70. Sprenger, M.; Dölle, N.; Schauwecker, F.; Raffler, M.; Ellersdorfer, C.; Sinz, W. Multiscale Analysis and Safety Assessment of Fresh and Electrical Aged Lithium-Ion Pouch Cells Focusing on Mechanical Behavior. *Energies* **2022**, *15*, 847. [CrossRef]
71. Gstrein, G.; Abbas, S.M.; Ewert, E.; Wenzl, M.; Ellersdorfer, C. Safety-Critical Influence of Ageing on Mechanical Properties of Lithium-Ion Pouch Cells. *Batteries* **2025**, *11*, 99. [CrossRef]

72. Abbas, S.M.; Gstrein, G.; Jauernig, A.D.; Schmid, A.; Michelini, E.; Hinterberger, M.; Ellersdorfer, C. Influence of Lithium Plating on the Mechanical Properties of Automotive High-Energy Pouch Batteries. *Batteries* **2025**, *11*, 330. [CrossRef]
73. Guo, Z.; Ma, Z.; Liu, J.; Zhao, W.; Wang, S.; Zhao, H.; Ren, L. Overcharging cycle aging-induced severe degradation of safety properties of lithium-ion pouch battery cells subjected to mechanical abuse. *Energy* **2025**, *320*, 135168. [CrossRef]
74. Xu, J.; Jia, Y.; Liu, B.; Zhao, H.; Yu, H.; Li, J.; Yin, S. Coupling Effect of State-of-Health and State-of-Charge on the Mechanical Integrity of Lithium-Ion Batteries. *Exp. Mech.* **2018**, *58*, 633–643. [CrossRef]
75. Lamb, J.; Orendorff, C.J. Evaluation of mechanical abuse techniques in lithium ion batteries. *J. Power Sources* **2014**, *247*, 189–196. [CrossRef]
76. Luo, H.; Jiang, X.; Xia, Y.; Zhou, Q. Fracture Mode Analysis of Lithium-Ion Battery Under Mechanical Loading. In Proceedings of the ASME 2015 International Mechanical Engineering Congress and Exposition, Houston, TX, USA, 13–19 November 2015. [CrossRef]
77. Wang, H.; Wu, Y.; Cao, Y.; Liu, M.; Liu, X.; Liu, Y.; Liu, B. Investigate the changes of aged lithium iron phosphate batteries from a mechanical perspective. *iScience* **2024**, *27*, 111300. [CrossRef] [PubMed]
78. Feinauer, M.; Abd-El-Latif, A.A.; Sichler, P.; Wohlfahrt-Mehrens, M.; Hölzle, M.; Waldmann, T. Effects of Main Aging Mechanism and State of Charge on the Safety of 21700 Li-Ion Battery Cells with Ni-Rich NMC Cathode. *J. Electrochem. Soc.* **2024**, *171*, 110524. [CrossRef]
79. Friesen, A.; Horsthemke, F.; Mönnighoff, X.; Brunklaus, G.; Krafft, R.; Börner, M.; Risthaus, T.; Winter, M.; Schappacher, F.M. Impact of cycling at low temperatures on the safety behavior of 18650-type lithium ion cells: Combined study of mechanical and thermal abuse testing accompanied by post-mortem analysis. *J. Power Sources* **2016**, *334*, 1–11. [CrossRef]
80. Li, Z.; Chen, J.; Lan, F.; Li, Y. Constitutive Behavior and Mechanical Failure of Internal Configuration in Prismatic Lithium-Ion Batteries under Mechanical Loading. *Energies* **2021**, *14*, 1219. [CrossRef]
81. Song, Y.; Bulla, M.; Patanwala, H.; Sahraei, E. Validation of Sahraei Failure Criterion on cylindrical and pouch Lithium-ion battery cells. *J. Energy Storage* **2024**, *94*, 112371. [CrossRef]
82. Schmid, A.; Pasquale, A.; Ellersdorfer, C.; Raffler, M.; Champaney, V.; Ziane, M.; Chinesta, F.; Feist, F. Mechanical Characterization of Li-Ion Cells and the Calibration of Numerical Models Using Proper Generalized Decomposition. In *ASME International Mechanical Engineering Congress and Exposition*; American Society of Mechanical Engineers: New York, NY, USA, 2023; Volume 7: Energy. [CrossRef]
83. Greve, L.; Fehrenbach, C. Mechanical testing and macro-mechanical finite element simulation of the deformation, fracture, and short circuit initiation of cylindrical Lithium ion battery cells. *J. Power Sources* **2012**, *214*, 377–385. [CrossRef]
84. Zhang, C.; Santhanagopalan, S.; Sprague, M.A.; Pesaran, A.A. Coupled mechanical-electrical-thermal modeling for short-circuit prediction in a lithium-ion cell under mechanical abuse. *J. Power Sources* **2015**, *290*, 102–113. [CrossRef]
85. Wang, L.; Yin, S.; Xu, J. A detailed computational model for cylindrical lithium-ion batteries under mechanical loading: From cell deformation to short-circuit onset. *J. Power Sources* **2019**, *413*, 284–292. [CrossRef]
86. Wang, H.; Kumar, A.; Simunovic, S.; Allu, S.; Kalnaus, S.; Turner, J.A.; Helmers, J.C.; Rules, E.T.; Winchester, C.S.; Gorney, P. Progressive mechanical indentation of large-format Li-ion cells. *J. Power Sources* **2017**, *341*, 156–164. [CrossRef]
87. Ren, D.; Hsu, H.; Li, R.; Feng, X.; Guo, D.; Han, X.; Lu, L.; He, X.; Gao, S.; Hou, J.; et al. A comparative investigation of aging effects on thermal runaway behavior of lithium-ion batteries. *eTransportation* **2019**, *2*, 100034. [CrossRef]
88. Abada, S.; Petit, M.; Lecocq, A.; Marlair, G.; Sauvant-Moynot, V.; Huet, F. Combined experimental and modeling approaches of the thermal runaway of fresh and aged lithium-ion batteries. *J. Power Sources* **2018**, *399*, 264–273. [CrossRef]
89. Waldmann, T.; Wohlfahrt-Mehrens, M. Effects of rest time after Li plating on safety behavior—ARC tests with commercial high-energy 18650 Li-ion cells. *Electrochim. Acta* **2017**, *230*, 454–460. [CrossRef]
90. Amiri, M.N.; Håkansson, A.; Burheim, O.S.; Lamb, J.J. Lithium-ion battery digitalization: Combining physics-based models and machine learning. *Renew. Sustain. Energy Rev.* **2024**, *200*, 114577. [CrossRef]
91. Das Goswami, B.R.; Abdisobbouhi, Y.; Du, H.; Mashayek, F.; Kingston, T.A.; Yurkiv, V. Advancing battery safety: Integrating multiphysics and machine learning for thermal runaway prediction in lithium-ion battery module. *J. Power Sources* **2024**, *614*, 235015. [CrossRef]
92. Finegan, D.P.; Tjaden, B.; Heenan, T.M.M.; Jervis, R.; Di Michiel, M.; Rack, A.; Hinds, G.; Brett, D.J.L.; Shearing, P.R. Tracking Internal Temperature and Structural Dynamics during Nail Penetration of Lithium-Ion Cells. *J. Electrochem. Soc.* **2017**, *164*, A3285–A3291. [CrossRef]
93. Li, L.; Chen, X.; Hu, R.; Wang, T.; Ji, H.; Yuan, Q.; Ji, Y.; Jiang, Z.; Liu, W.; Zheng, W. Aging Mechanisms and Thermal Characteristics of Commercial 18650 Lithium-Ion Battery Induced by Minor Mechanical Deformation. *J. Electrochem. Energy Convers. Storage* **2021**, *18*, 021010. [CrossRef]

94. Wang, Z.; Zhao, Q.; Yu, X.; An, W.; Shi, B. Impacts of vibration and cycling on electrochemical characteristics of batteries. *J. Power Sources* **2024**, *601*, 234274. [CrossRef]
95. *GB 38031-2025*; Electric Vehicles Traction Battery Safety Requirements. State Administration for Market Regulation, Standardization Administration of China: Beijing, China, 2025.

Disclaimer/Publisher's Note: The statements, opinions and data contained in all publications are solely those of the individual author(s) and contributor(s) and not of MDPI and/or the editor(s). MDPI and/or the editor(s) disclaim responsibility for any injury to people or property resulting from any ideas, methods, instructions or products referred to in the content.